ENTANGLEMENT AND CORRELATION PROPERTIES OF EXCITON-POLARITONS IN SEMICONDUCTOR MICROCAVITIES

A thesis

submitted in fulfilment

of the requirements for the degree

of

Magister in physics

at

Universidad Nacional de Colombia

by

DANIEL GUSTAVO SUÁREZ FORERO

Under the advise of

Herbert Vinck Posada, Dr.
Grupo de Óptica e Información Cuántica
Departamento de Física
Facultad de Ciencias

UNIVERSIDAD NACIONAL DE COLOMBIA

November 2015
Bogotá-Colombia

A quienes debo todo...
Nubia, Álvaro y Juliana

ABSTRACT

Polariton, the quasiparticle emerging from the strong coupling between light and matter in semiconductor microcavities has shown to be a good candidate for applications in quantum information processing devices, and in the last years has become the cornerstone of the solid state realization of quantum computation. The necessary condition that endows these protocols with remarkable advantages over their classical counterparts is the so called entanglement or non separability of states, an exclusive property of quantum mechanical systems.

The present thesis is a compilation of three theoretical works about the quantum properties of semiconductor microcavity-quantum dot systems. In each case a model of a two level system interacting with a single electromagnetic mode of the microcavity via dipolar interaction is used.

First of all, we study the case of a single quantum dot embedded in an optical microcavity by using a dissipative Jaynes-Cummings model. Two non coherent processes are considered: photon leakage through the cavity walls and exciton pumping. The steady state of the system is calculated in a master equation formalism, then mixedness and entanglement are quantified through linear entropy and negativity, respectively. In particular we find the set of parameters that maximizes light-matter entanglement and purity in the system. Then, an extension to the multiple non interacting quantum dots case is made.

In the second work, we analyze the possibility of change the incoherent exciton pumping for a non dissipative matter pumping mechanism in order to study if it favors the non separability of the subsystems. Again, we find the set of parameters that maximize light-matter entanglement and purity of the system in its steady state. A comparison with a maximally entangled (Bell) state is performed with aid of the fidelity criteria.

Finally, an extension to the case of interacting quantum dots is made by using a Tavis-Cummings model with a dot-dot interaction term. As a first approach to the complete problem, the entanglement of the eigenstates of the hamiltonian is quantified through the concurrence criteria.

PUBLICATIONS

The ideas developed in this work have been presented in the following events:

- International Workshop on Quantum Coherence and Decoherence, Cali, Colombia
- Quantum Optics VI Conference, Piriápolis, Uruguay
- IV Quantum Information School, Paraty, Brasil
- 1st Workshop on Metamaterials and Photonic Crystals, Armenia, Colombia
- Research in Optical Science Congress, Berlín, Alemania
- International workshop on quantum coherence and decoherence II, Medellín, Colombia
- Quantum Optics VII, Mar del Plata, Argentina
- V Quantum Information School, Paraty, Brasil

And in the following references

- D. G. Suarez Forero and H. Vinck-Posada, "Effects of the Von-Förster interaction in the emission spectra of a microcavity-quantum dots system", in Research in Optical Sciences , OSA Technical Digest (online) (Optical Society of America), paper JW2A.30.
- Revista Colombiana de Física, Vol 44, Dinámica de un sistema de microcavidad–punto cuántico: más allá del régimen excitónico I
- Revista Colombiana de Física, Vol 44, Dinámica de un sistema de microcavidad–punto cuántico: más allá del régimen excitónico II
- arXiv:1205.2719. D. G. Suárez-Forero, G. Cipagauta, H. Vinck-Posada, K. M. Fonseca-Romero and B. A. Rodríguez. Can the exciton–polariton regime be defined by its quantum properties?

AGRADECIMIENTOS

La primera persona a quien quiero agradecer es Herbert Vinck Posada, quien desde mis primeros años de formación profesional me tendió la mano y se convirtió en un guía a través de todo este proceso, que hoy permite la realización de esta tesis, de la cual, él es asesor, el mejor asesor que pude haber encontrado.
A mis padres y hermana, por brindarme apoyo incondicional todos estos años y permitirme la dedicación exclusiva a mi formación como físico, así como por brindarme un ambiente sano y tranquilo, propicio para la realización de todos mis estudios.
Agradezco además al Grupo de Óptica e Información Cuántica de la Universidad Nacional de Colombia, conformado por los profesores Karen Fonseca, Rafael Rey y Herbert Vinck, quienes me dieron espacios académicos de discusión y formación, así como apoyo económico para mi asistencia a eventos y escuelas que permitieron reflexiones e intercambios de ideas que hicieron grandes aportes a mi carrera. Agradezco también a mis compañeros y amigos, quienes también pertenecen al grupo y de quienes recibí invaluable retroalimentación sobre mi trabajo, nuevas ideas y una buena amistad.
A toda mi familia por su colaboración constante y su interés en el transcurso de mi carrera.
Al departamento de Física de la Universidad Nacional de Colombia por permitirme estar al lado de destacados físicos, de quienes se me permitió ser alumno en estos años. Estoy profundamente agradecido con la institución y hoy me siento orgulloso y satisfecho de haber sido formado aquí, tanto como en mi carrera profesional como en mi maestría.

Agradezco también al proyecto de Colciencias "*Exploración y modelación de la iridiscencia en especies colombianas*", código 110156933525, a cargo del profesor Herbert Vinck Posada, por financiamiento parcial de las labores de investigación.

CONTENTS

Part I

INTRODUCTION

1 INTRODUCTION

When an optical emitter is placed inside a cavity, the lifetimes of its optical modes are drastically affected, a phenomenon known as the Purcell effect [1]. This effect, combined with a constant energy exchange between the electromagnetic mode of the cavity and the emitter, can drive the system into a regime referred to as "Strong coupling", a situation in which an emitted photon has a greater probability of being reabsorbed than of scape out of the cavity[2]. The physics of systems in strong coupling is correctly described by the theoretical model developed by Jaynes and Cummings[3, 4]. This regime is of great interest, thanks to the new quantum states that take place on it. After being achieved in atomic and superconducting systems[5, 6], the technology of semiconductor nanostructures reached the capability of sustain strong coupling[7, 8], bridging the era of quantum information processing to solid state devices[9, 10, 11].

1.1 THE JAYNES-CUMMINGS MODEL FOR MICROCAVITY-QUANTUM DOT SYSTEMS

Since the discovery of strong coupling in quantum dot-microcavity systems[2, 7], a very promising research area emerged. The full quantization of the energy states of an electron provided by its 3D confinement inside a quantum dot (also known as artificial atom) make these systems very interesting from a theoretical point of view (given that they allow to study quantum mechanics in a very fundamental level) as well as from a technological one (due to their micrometric size these systems have a great implementability)[12, 13].

In general, a microcavity is a semiconductor heterostructure able to confine light by Bragg reflection and total internal reflection [14]. Solid state growth methods like chemical vapor deposition and molecular beam epitaxy[15, 16] allow to confine light in volumes of the order of 1 μm^3 [14]. On the other hand, if the cavity has a quantum dot embedded inside, the multiple absorptions and emissions drive the system into the strong coupling regime.

The question of whether the strong coupling regime of a microcavity-quantum dot system is classical or quantum, remained open until 2007, when it was experimentally shown that this phenomenon has a quantum nature[17, 18]. While some features of the strong coupling regime can be correctly described by using a semiclassical theory[19], the antibunching measured in a Hanbury-Brown and Twiss configuration [20] is an unambiguous proof of the quantum nature of the strong coupling in the sense that only one emitter is interacting with the resonator mode[21]. We will make a more detailed study of this

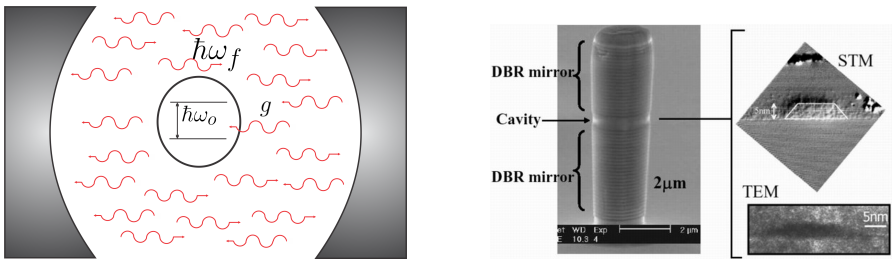

Figure 1: (Color online) Left: Schematic picture of the Jaynes-Cummings model. A two-level system interacting with a mode of the electromagnetic field. Right: Picture of a photonic micropillar. TEM (Transmission Electron Micrograph) and STM (Scanning Tunneling Micrograph) pictures allow to see the quantum dot growth inside the microcavity. This is the condensed matter realization of the Jaynes-Cummings model. Right picture taken by the *Low Dimensional Structures and Devices Group* at *The University of Sheffield*.

in section 1.3.

The most simple full quantum model that describes a cavity with a confined electromagnetic mode interacting with a single quantum dot, is the Jaynes-Cummings model[3, 4, 22]. It considers a single mode of the electromagnetic field ($|n\rangle$) interacting with a two level system ($|G\rangle$ and $|X\rangle$). The employed Hamiltonian is given by (in units $\hbar = 1$):

$$\hat{H} = \omega_C \hat{a}^\dagger \hat{a} + \omega_o \hat{\sigma}^\dagger \hat{\sigma} + g(\hat{a}\hat{\sigma}^\dagger + \hat{a}^\dagger \hat{\sigma}) \tag{1}$$

Where ω_C is the energy of the electromagnetic field, $\hat{a}$ ($\hat{a}^\dagger$) is the common annihilation (creation) operator, ω_o is the transition energy of the two level system, the operator $\hat{\sigma} = (\hat{\sigma}^\dagger)^\dagger$ is given by $|G\rangle\langle X|$ and g is the light-matter interaction energy (also known as Rabi frequency) [3, 4]. Figure 1 depicts a system of a cavity with an atom (or an artificial atom) inside together with the picture of an actual micropillar taken by the Low Dimensional Structures and Devices Group of The University of Sheffield, one of the referent groups in this kind of systems. Micropillars are unidimensional photonic crystals able to confine light by Bragg reflection inside a defect that becomes a cavity [23]. When a quantum dot is embedded in the cavity, and if its transition energy is near to the energy of the cavity mode, light-matter interaction takes place [24].

1.2 ANTICROSSING AND ENTANGLEMENT

One feature of the systems in which the Jaynes-Cummings model is valid, is the so called *Anticrossing*, a rupture of the degeneration of the system's energy in the case of resonance between light and matter.

Theoretically, it corresponds to the eigenvalues of the energy operator (1). In units $\hbar = 1$ they are given by:

$$E_{\pm}(n) = \left(n + \frac{1}{2}\right)\omega_C \pm \sqrt{\Delta^2 + 4g^2(n+1)} \tag{2}$$

Where $\Delta = \omega_C - \omega_o$ is the energy detuning between the quantum dot and the cavity, and n is the excitation manifold, a preserved quantity, given that the operator $\hat{N} = \hat{a}^\dagger\hat{a} + \hat{\sigma}^\dagger\hat{\sigma}$ commutes with the energy operator $\hat{H}$.
Experimentally, the anticrossing is measured through the emission peaks of the system, by recording the energy in which the emission is maximum. The upper left panel of figure 2 shows the theoretical eigenvalues of the Jaynes-Cummings Hamiltonian in arbitrary units[22] together with the bare energies, i.e. the energy of the electromagnetic field (ω_C) and the energy of transition in the quantum dot (ω_o), which are the eigenenergies of the system in the absence of interaction ($g = 0$). In the upper right panel of the same figure, it is shown the original picture from the first experimental proof of strong coupling in microcavity-quantum dots systems, reported in [7]. It shows the emission spectra for different temperatures, i.e. for different detunings, given that the emission energy of a quantum dot depends on its temperature. Each peak on the emission spectra is associated with an eigenenergy of the system, so the fact that there are two peaks for any Δ means that the energy degeneracy has been removed, and the system has been pushed into the strong coupling regime. The lower panels record the position of the emission peaks for each temperature (detuning), that is the experimental realization of the upper left picture. Panel **a** shows a behavior as the one described by the blue lines (the behavior of the system when interaction takes place), while panel **b** shows the behavior of the system in the absence of light-matter interaction, which is the one described by the black lines.

Notice that in weak coupling ($g = 0$), the eigenvalues are degenerated when the energy of the electromagnetic mode is the same as the transition energy of the quantum dot, however, in strong coupling, the system has not the energy of the cavity and neither the energy of the quantum dot: two new states, known as dressed states or polaritons take place [2]. In the absence of dissipation these polaritonic states can be written in general as:

$$\begin{aligned} |n,+\rangle &= \sin\theta\,|G,n\rangle + \cos\theta\,|X,n-1\rangle \\ |n,-\rangle &= \cos\theta\,|G,n\rangle - \sin\theta\,|X,n-1\rangle \end{aligned} \tag{3}$$

Where the angle θ is defined through the relation[22]

$$\tan\theta = \frac{2g\sqrt{n+1}}{\Delta}$$

One of the most remarkable features of this model is the matter light entanglement of its eigenstates. Notice that for any $g \neq 0$ and $\Delta < \infty$ they are not separable; this light matter entanglement make

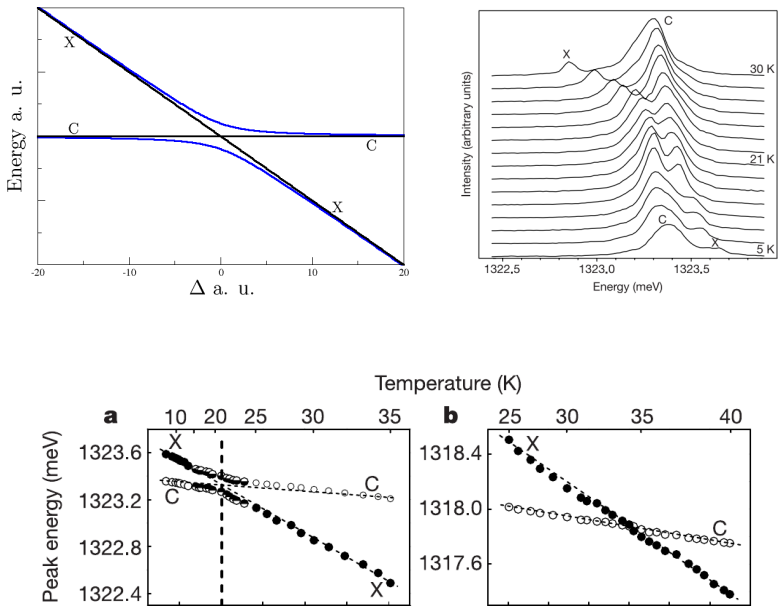

Figure 2: (Color online) Upper left panel: theoretical eigenenergies of the Jaynes-Cummings Hamiltonian. The black line is for a system in the hamiltonian weak coupling regime, while the blue one is for a system in strong coupling. Upper right panel: emission intensity of a microcavity (C)-quantum dot (X) system. The matter transition energy is modified by increasing sample's temperature. The emission spectra presents always two peaks, this means that there is never a degeneration in the energies i.e. system's emission presents anticrossing. Lower panel: Position of the emission peaks for each temperature for systems in strong (a) and weak coupling (b). Notice that the lower panel is very similar to the theoretical calculations. Upper right and lower pictures are taken from: Nature, 432, Nov. 2004 [7]. In fact, this is the first experimental proof of strong coupling between light and matter in microcavity-quantum dot systems. These graphics are comparable with the upper left because, despite dissipation, the system preserves most of the features of its hamiltonian behavior.

polaritons one of the cornerstones of the solid state realization of quantum information processing[11, 21].

One important concern is about the degree of non separability of a state, in the sense of how near is the state of being factorable. For example, the state $|\phi_1\rangle = \sqrt{0.99}\,|G, n\rangle + \sqrt{0.01}\,|X, n-1\rangle$ is more similar to a factorable state than $|\phi_2\rangle = \sqrt{0.5}\,|G, n\rangle + \sqrt{0.5}\,|X, n-1\rangle$. There are multiple ways to quantify the degree of entanglement of a system, and this is still an active research field, however, in this thesis we use two quantities: "Negativity" or "Peres criteria", defined as the sum of the negative eigenvalues of the partial transpose of the density operator $\hat{\rho}$ [25, 26] and "Concurrence", a quantity given by:

$$C(\hat{\rho}) = max(0, \lambda_1 - \lambda_2 - \lambda_3 - \lambda_4) \tag{4}$$

Where λ_i are the eigenvalues, in decreasing order, of the hermitian operator

$$R = \sqrt{\sqrt{\hat{\rho}}\,[(\hat{\sigma}_y \otimes \hat{\sigma}_y)\,\hat{\rho}^*\,(\hat{\sigma}_y \otimes \hat{\sigma}_y)]\,\sqrt{\hat{\rho}}} \tag{5}$$

Where $\hat{\sigma}_y$ is the y Pauli matrix and $\hat{\rho}^*$ is the density operator with its components conjugated[26, 27].

If we study the dependence of the non separability with the detuning Δ for the eigenstates of the Jaynes-Cummings hamiltonian by using the negativity, we will obtain figure 3. It can be seen that for resonance the system is maximally entangled, it means that the state will have the form

$$|\psi\rangle = \frac{1}{\sqrt{2}}(|G, n\rangle \pm |X, n-1\rangle)$$

Which is precisely a Bell state, the most entangled state achievable in a qubit-qubit system. This is a very desirable effect, with many technological applications such us quantum cryptography, quantum teleportation, logic gates for quantum computation, etc [28]. As the energy difference between the emitter and the light increases, the state becomes more separable, and when Δ is too large, the system loses its entanglement due to the absence of interaction.

1.3 CORRELATION

In the 1960s, Glauber constructed a quantum coherence theory parallel to the classical one[22]. He used the so called "correlation function of order M", a function related with the M first statistical moments of the field's photon number distribution; a knowledge of the exact photon number distribution implies the knowledge of the infinite correlation functions and viceversa [29]. This function relates the electromagnetic field in M space-time coordinates $(\vec{r}_1, t_1, \vec{r}_2, t_2, ..., \vec{r}_M, t_M)$.

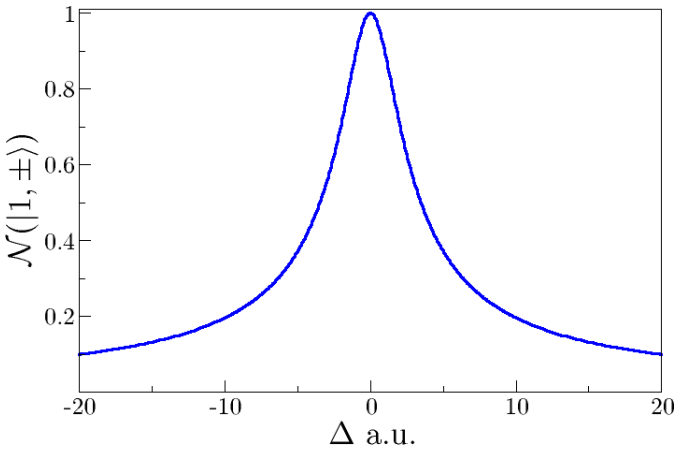

Figure 3: (Color online) Negativity of the eigenstates of Jaynes Cummings Hamiltonian as a function of the energy difference between light and matter (detuning). For $\Delta = 0$ the state is maximally entangled, and as Δ increases the system becomes more separable due to the absence of interaction.

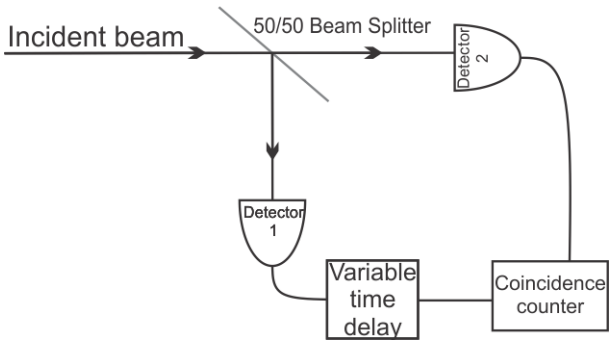

Figure 4: Hanbury-Brown and Twiss experimental setup to measure $g^{(2)}(\tau)$. An incident beam is splitted and each arm is sent to detectors. One of the arms is delayed and then sent to a coincidence counter.

A widely used quantity is the second order correlation function, which is related with the probability that an active media has of emitting two photons one after the other with a time delay τ between them. For a single mode of the electromagnetic field, its normalized version is given by[30]:

$$g^{(2)}(t,\tau) = \frac{\langle \hat{a}^\dagger(t)\hat{a}^\dagger(t+\tau)\hat{a}(t+\tau)\hat{a}(t)\rangle}{\langle \hat{a}^\dagger(t)\hat{a}(t)\rangle^2} \tag{6}$$

Experimentally, $g^{(2)}$ can be measured through a Hanbury-Brown and Twiss setup[20]. A schematic picture of this experiment is shown in figure 4. It is composed by a half-half beam splitter that divides the incident light in two arms. On each arm a photodetector is placed. One of the photodetectors is able to introduce a time delay in the detection, and at the end, the signal is recorded in a coincidence counter.

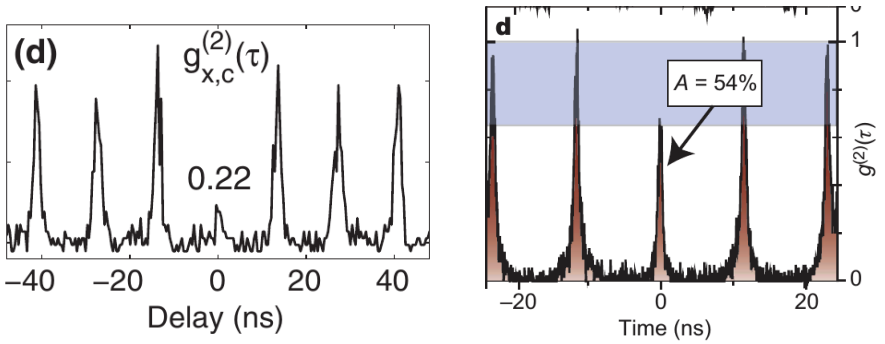

Figure 5: (Color online) Pictures from the experimental proof of the quantum nature of strong coupling in mirocavity-quantum dot systems. The second order correlation function $g^{(2)}(\tau)$ has a reduction at zero delay, which means that photons are being emitted by one at a time and the resonator mode is interacting with a single quantum dot. The picture in the left panel is taken from [18] and the one in the right panel is taken from [17].

At zero delay $g^{(2)}$ is reduced to:

$$g^{(2)} = \frac{\langle \hat{a}^\dagger \hat{a}^\dagger \hat{a} \hat{a} \rangle}{\langle \hat{a}^\dagger \hat{a} \rangle^2}$$

This quantity is of interest given that it is possible to link it with statistical properties of the field such us variance ($\Delta n^2 = \langle (n - \langle n \rangle)^2 \rangle$) and mean number of photons ($\langle n \rangle$). They can be related by:

$$g^{(2)} = 1 + \frac{\Delta n^2 - \langle n \rangle}{\langle n \rangle^2}$$

For some specific states its values are well known. For a Fock state of n photons ($|n\rangle$) $g^{(2)}$ is always less than 1, for a coherent state ($|\alpha\rangle$) its value is always one, and for a thermal state $g^{(2)} = 2$ [30]. This was used by Imamoglu et. al. and Yamamoto et. al. to experimentally probe in the same year (2007) the quantum nature of strong coupling in microcavity-quantum dot systems[17, 18]. For a quantum state $|n\rangle$, $g^{(2)}(0) < 1$, and in particular, for the state $|1\rangle$, $g^{(2)}(0) = 0$, this means that only one single photon is being emitted at the same time, hence no coincidences at zero delay will be recorded. Their results are shown in figure 5, and this is an unambiguous proof of the quantum nature of the strong coupling in semiconductor microcavities with quantum dots embedded, in the sense that only one emitter is interacting with the cavity mode.

The greater correlation functions ($g^{(n)}$) give more information about the statistics of the field and its degree of coherence. One says that a field is nth order coherent if the first n correlation functions are 1. A fully coherent state satisfies the condition $|g^{(n)}| = 1$ for all n.
In the case of a single mode of the field the normalized coherence function of order n is given by:

$$g^{(n)} = \frac{\langle \hat{a}^{\dagger n} \hat{a}^n \rangle}{\langle \hat{a}^\dagger \hat{a} \rangle^n} \tag{7}$$

A more detailed description of this topic can be found in chapter 19 of reference [31].

1.4 OPEN SYSTEMS AND MASTER EQUATION

When a system is immersed into a reservoir, the total dynamics can, in principle, still be described by coherent dynamics. However this is impractical and unnecessary given that the interest usually lies on the system instead of its reservoir. It is possible then to ignore the degrees of freedom of the reservoir by keeping only its effects on the system of interest [30]. The price we have to pay is the lost of coherence in the system: the state will not be described anymore by a vector but by an operator: the density operator [32]. The dynamics will not be described anymore by the Schrödinger equation (or Liouville Von-Neumann's), but by a new formalism known as "Master equation" [30].
The formalism can be used to describe systems under the effects of loss of coherence due to different mechanisms: photon leakage through cavity walls, spontaneous emission, external pumping, dephasing, etc. The density operator's dynamics is given now by:

$$\frac{d\hat{\rho}}{dt} = i[\hat{\rho}, \hat{H}] + \sum_i \hat{\mathcal{L}}_i(\hat{\rho}) \tag{8}$$

Where $\hat{\rho}$ is the density operator, $\hat{H}$ is the hamiltonian and $\hat{\mathcal{L}}$ are the Liouvillian operators, which take the information about the incoherent processes. Each dissipative process has a Liouvillian operator (or Linbland term) associated. The derivation of these terms can be done, principally by two methods[30]: the first one considers dissipation as a coupling to a bath of oscillators, and tracing out the degrees of freedom of the reservoir, only the information of the system is kept. This approach is described in references [33] and [34]. The second path for the derivation of the master equation and Linbland terms is based on Monte Carlo methods and quantum jumps. In references [22] and [35] this is the preferred approach.

Quantum dot-microcavity systems usually work at cryostat temperatures, where the most relevant dissipative channel is the photon leakage through the cavity walls. To compensate this mechanism, it is necessary to perform an incoherent exciton pumping in order to keep the dynamics and reach non trivial steady states. Therefore, these two processes dominate the incoherent behavior in these kind of systems. Mathematically, photon scape and exciton pumping are given respectively by the Liouville operators[33]:

$$\hat{\mathcal{L}}_\kappa(\hat{\rho}) = \frac{\kappa}{2}(2\hat{a}\hat{\rho}\hat{a}^\dagger - \hat{a}^\dagger\hat{a}\hat{\rho} - \hat{\rho}\hat{a}^\dagger\hat{a}) \tag{9}$$

$$\hat{\mathcal{L}}_P(\hat{\rho}) = \frac{P}{2}(2\hat{\sigma}^\dagger\hat{\rho}\hat{\sigma} - \hat{\sigma}\hat{\sigma}^\dagger\hat{\rho} - \hat{\rho}\hat{\sigma}\hat{\sigma}^\dagger) \tag{10}$$

To understand better the effect of these mechanisms on the system, we can study the ladder of states, a scheme in which the transitions

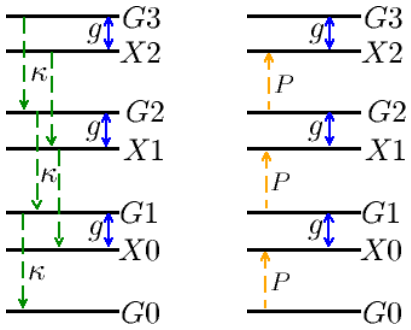

Figure 6: (Color online)Ladder of states for the Jaynes-Cummings model under two incoherent mechanisms: Photon leakage through the cavity walls (left) and incoherent exciton pumping (right). The blue arrows show the transitions generated by the hamiltonian interaction while the green and orange arrows show the transitions generated by the photon escape and exciton pumping, respectively.

generated by pumping and dissipation are depicted. This is shown in figure 6. It shows how the dissipation affects the bare states of the system. One important feature is that dissipation, unlike hamiltonian dynamics[22], is able to generate transitions between states of different excitation manifolds in the Jaynes-Cummings model, so for an open system this is not a preserved quantity anymore.

1.5 TWO QUANTUM DOTS-MICROCAVITY SYSTEM

When the density of quantum dots inside a microcavity is high enough, they are able to interact via two mechanisms: the transfer of an electron between quantum dots by tunneling[36], and the transfer of the excitation via an intermediate virtual photon, a mechanism known as Förster interaction[37, 38]. On each case the description of the system can be done by means of the same hamiltonian[39, 40] (in units $\hbar = 1$):

$$\hat{H} = \omega_C \hat{a}^\dagger \hat{a} + \sum_{i=1}^{2} \left[\omega_{Xi} \hat{\sigma}_i^\dagger \hat{\sigma}_i + g_i \left(\hat{\sigma}^\dagger \hat{a} + \hat{\sigma} \hat{a}^\dagger \right) \right] + T_e \left(\hat{\sigma}_1 \hat{\sigma}_2^\dagger + \hat{\sigma}_1^\dagger \hat{\sigma}_2 \right) \tag{11}$$

Where ω_C is the energy of the cavity mode, ω_{Xi} the transition energy of the exciton, g_i is the dipole interaction strength for each quantum dot, T_e is the strength of interaction between the quantum dots, $\hat{a}$ is the annihilation operator for the electromagnetic field and $\hat{\sigma}_i$ is the fermionic annihilation operator for the i-th quantum dot. Given that the parameters employed in the description of the problem are typical from the former mechanism, we are focusing on it in the rest of the section. We show the approach used in references [36, 39, 41] and [42]

When an exciton is created inside a quantum dot it remains in the conducting band of the structure, however, if another potential well

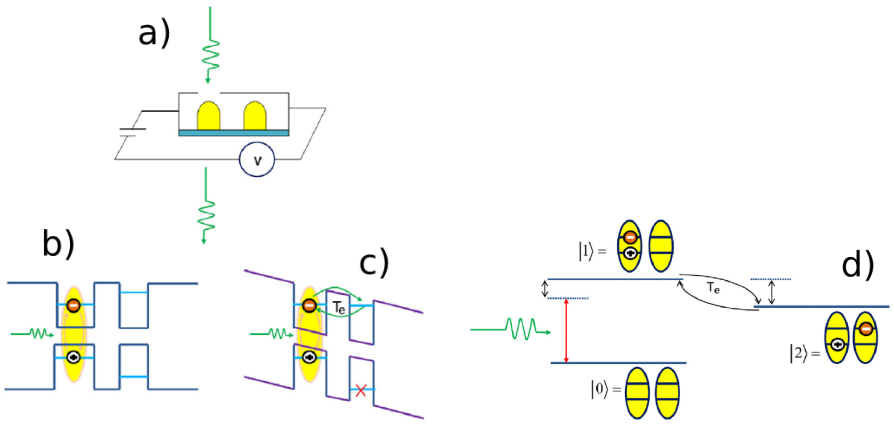

Figure 7: (Color online) a): setup scheme. The cavity mode drives strongly the left quantum dot. V is the bias voltage that controls the tunneling barrier height. b) and c): Schematic of the band structure without and with an applied voltage, respectively. In panel c) the conduction band levels get into resonance, increasing their coupling, while the valence bands become more off-resonance, which decouples those levels. d): Energy levels of the double quantum dot system. Figure taken from reference [39]

(quantum dot) is placed near, the probability of tunneling to the second quantum dot does not vanish. The electron can cross the potential barrier and get the second quantum dot while still being bounded to the hole in the first quantum dot, giving rise to an "indirect exciton" state. Experimentally, the tunneling barrier can be controlled by placing a gate electrode between the quantum dots. Under these conditions the system can be simplified to a three-level system: the ground state (no excitation in the system) $|0\rangle$, the exciton state $|1\rangle$, corresponding to an exciton inside one of the quantum dots, and the indirect exciton state $|2\rangle$, with the electron in one dot and the hole in another. A full scheme of the system is depicted in figure 7.

This configuration brings control on the coupling strength between the quantum dots, given that a gate voltage tune the energy of the conduction band in the quantum dot, the greater the detuning between the bands, the smaller the coupling between the quantum dots. In general, the quantum dots are asymmetric, so in the absence of a gate voltage the conduction bands are out of resonance, and hence, the electron tunneling between the quantum dots is very weak. This voltage enhances significantly the tunneling probability and additionally increases the energy difference between the valence bands, thus the hole tunneling can be neglected in the model.

At this point, we have discussed all the necessary elements to address the three problems of interest. The results are showed in chapters 2, 3 and 4. Then, in chapter 5 we make an overview and give some conclusions. Finally, in chapters 6 and 7 we present two appendices, making a deeper discussion about the obtainment of some of the results displayed in the former chapters.

Part II

RESULTS

2

ENTANGLEMENT PROPERTIES OF QUANTUM POLARITONS

Polariton, the quasiparticle emerging from the strong coupling between light and matter in microcavity-quantum dot systems is one of the cornerstones of the condensed matter realization of quantum information processing[11, 21]. However, its nature differs substantially from the paradigm of trapped atoms in optical cavities[43] and dissipation is of a fundamental character as much as hamiltonian dynamics itself, so the effect of incoherent processes on the entanglement, correlation and purity of polaritons, arises as a natural question[44, 45]. The aim of this work is to study these properties in a master equation formalism[33] by considering two dissipative effects: photon escape through the cavity walls and incoherent exciton pumping, the two most relevant effects at cryostat temperatures. In particular, entanglement is measured by using the negativity criteria, light correlations are studied by computing the second and third order correlation functions at zero time delay, and purity is quantified by the linear entropy of the density operator.

2.1 THEORETICAL FRAMEWORK

The model considers a two level atom interacting with a single electromagnetic mode with strength g, photons are able to escape at a rate κ due to imperfections on the cavity and an incoherent exciton pumping is performed at a rate P. Figure 8 shows an schematic picture of the system.

The quantum dot has two accessible levels $|G\rangle$ and $|X\rangle$ and the electromagnetic field ($|n\rangle$) has an energy ω_C. Photons escape at a rate κ and excitons are pumped at a rate P. There is a detuning Δ between the energies of the field and the quantum dot. The Hamiltonian of the system is given by (in units $\hbar = 1$):

$$\hat{H} = \omega_C \hat{a}^\dagger \hat{a} + (\omega_C - \Delta)\hat{\sigma}^\dagger \hat{\sigma} + g(\hat{a}\hat{\sigma}^\dagger + \hat{a}^\dagger \hat{\sigma}) \tag{12}$$

Where dipole and rotating wave approximations have been done, $\hat{a} = (\hat{a}^\dagger)^\dagger$ is the annihilation operator for the cavity mode and $\hat{\sigma} = (\hat{\sigma}^\dagger)^\dagger = |G\rangle\langle X|$ is the fermionic annihilation operator for the quantum dot. The dynamics of the system is governed by the master equation:

$$\frac{d\hat{\rho}}{dt} = i[\hat{\rho}, \hat{H}] + \frac{1}{2}P(2\hat{\sigma}^\dagger \hat{\rho}\hat{\sigma} - \hat{\sigma}\hat{\sigma}^\dagger \hat{\rho} - \hat{\rho}\hat{\sigma}\hat{\sigma}^\dagger) + \frac{1}{2}\kappa(2\hat{a}\hat{\rho}\hat{a}^\dagger - \hat{a}^\dagger \hat{a}\hat{\rho} - \hat{\rho}\hat{a}^\dagger \hat{a}) \tag{13}$$

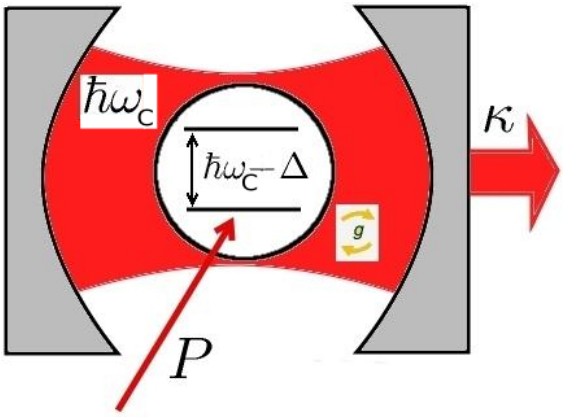

Figure 8: (Color online) Schematic picture of a two level atom interacting with a mode of the electromagnetic field inside a microcavity. Three important parameters are depicted: (g) light-matter interaction strength, (P) incoherent exciton pumping and ($\kappa = \omega/Q$) photon leakage rate due to imperfections on the cavity. ω is the field frequency and Δ is its energy detuning with the quantum dot.

Our approach focuses on the steady state of the system $\hat{\rho}_{ss}$. The basic assumption is that polariton lifetime is much longer than the time required to reach the asymptotic solution[46, 47]. In general, the steady state is a function of the dissipation rates κ and P, the matter light coupling constant g and the detuning Δ. Unless stated otherwise, the solution is obtained by setting $\omega_C = 1$ eV, $g = 0.1$ meV and $\kappa = 5 \times 10^{-3}$ meV. Δ and P are varied in ranges similar to those of current experiments. A more detailed explanation about the obtainment of the density operator $\hat{\rho}_{ss}$ is given in the appendix A (chapter 6).

2.2 LIGHT-MATTER ENTANGLEMENT AND PURITY

Linear entropy and negativity are computed to quantify purity and entanglement, respectively. The former, defined as $S_L(\hat{\rho}) = 1 - Tr(\hat{\rho}^2)$, vanishes for pure states and is maximum for maximally mixed states. The latter is defined as $\mathcal{N}(\hat{\rho}) = 2\sum_{\lambda<0}|\lambda|$, where λ denotes the eigenvalues of the partial transpose of $\hat{\rho}$.

Negativity and linear entropy are depicted in Fig. 9 for different detuning conditions ($\Delta = 0$, $\Delta = g$, $\Delta = 2g$, $\Delta = 3g$, $\Delta = 7g$ and $\Delta = 10g$) and as a function of the pumping power P. As expected from a physical point of view, the maximum of the negativity occurs at $P = \kappa$, when gain and losses exactly compensate. At this point the system presents a maximum of entanglement that coincides with a local minimum in the degree of mixedness. The dependence on the detuning shows instead a non-monotonic behavior, with a maximum value of $\mathcal{N} \approx 0.32$ for $\Delta \approx 3g$, corresponding to the minimum of

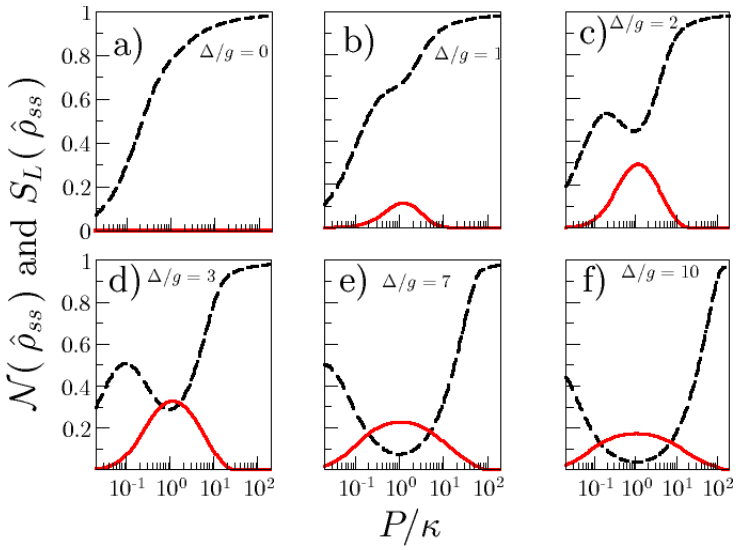

Figure 9: (Color online) $\mathcal{N}(\hat{\rho}_{ss})$ (continuous red line) and $S_L(\hat{\rho}_{ss})$ (dashed black line) as a function of the incoherent exciton pumping P, for $\kappa = 5 \times 10^{-3}$ meV and (a) $\Delta = 0$, (b) $\Delta = g$, (c) $\Delta = 2g$, (d) $\Delta = 3g$, (e) $\Delta = 7g$ and (f) $\Delta = 10g$. Note that for $\Delta \neq 0$ the maximum of $\mathcal{N}(\hat{\rho}_{ss})$ always corresponds to a local minimum of $S_L(\hat{\rho}_{ss})$ when $\kappa = P$.

the linear entropy, $S_L \approx 0.29$. Fixing the condition of $P = \kappa$, we plot in Fig. 10 the behavior of the linear entropy and the negativity as a function of the detuning. As mentioned before, the excitation number ($\hat{N} = \hat{a}^\dagger\hat{a} + \hat{\sigma}^\dagger\hat{\sigma}$) symmetry associated with the hamiltonian 12, is broken in the time evolution because of the incoherent processes, therefore, we can not label the steady state with a single eigenvalue of $\hat{N}$.

From figure 10 it is possible to identify three different regimes: if the subsystems are in resonance (or near this condition), the interaction, combined with dissipation, produce a very mixed state $S_L \approx 0.75$, therefore no entanglement is achievable in this conditions[48]. $\mathcal{N}$ then vanishes in the interval $-g \lesssim \Delta \lesssim g$. On the other hand, for large detunings matter and light do not couple, so the interaction strength is not enough to generate entanglement. The quantum dot is saturated due to the absence of interaction and exciton pumping, driving the system into the non entangled, pure state $|X0\rangle$. The entropy takes low values in this regime but the negativity decreases as well. The best condition is then the one in which the entropy is low enough to do not destroy the quantum properties of the system, and the interaction is high enough to generate non-separable states. This is the case for $\Delta \approx 3g$. At this point there is a maximum in the negativity that coincides with a local minimum in linear entropy. Although the density matrix is not pure, the system has a probability of 84% of being in the non-separable state $0.29\,|G1\rangle - 0.96\,|X0\rangle$. A diagonalization of the density matrix shows the steady state for each detuning, as reported in Table 1. Details on this diagonalization are given in appendix A

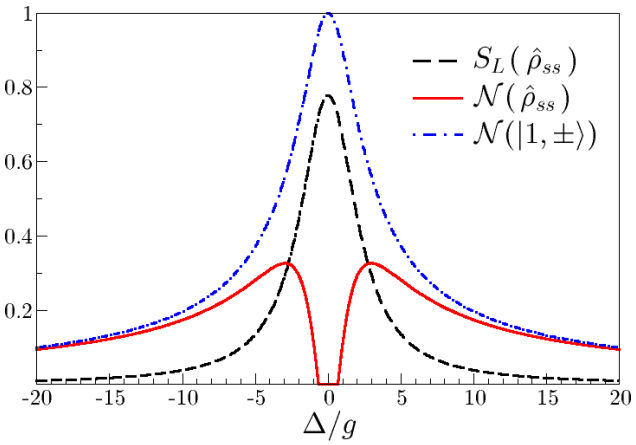

Figure 10: (Color online) Linear entropy (dashed black line) and negativity (continuous red line) of the steady state of the system $\hat{\rho}_{ss}$, and negativity of polaritons of the excitation manifold Λ_1 (dashed-dotted blue line) as a function of Δ for $P = \kappa = 5 \times 10^{-3}$ meV.

(chapter 6). For $\Delta = 0$ the state is a non-coherent superposition of entangled and separable states. At $\Delta = 20g$ the system has a high degree of purity (a probability of 99.5%) but is separable, due to saturation. In the mid region ($\Delta = 3g$) the competition of these effects generate an entangled state with probability 83.7%.

Fig. 11 compares the steady state of the system with pure polaritonic states defined as the eigenstates of $\hat{H}$ given by equation 3, using the sequence of non-zero fidelities $F_{n\pm} = \sqrt{\langle n \pm |\hat{\rho}_{SS}|n\pm\rangle}$[49]. For small values of P (Fig.11a) ρ_{G0G0}, the population of the state without polaritons, is much larger than the other populations. In this case, only F_1 does not vanish –it is relatively small, though–. For $P = \kappa$ (Fig.11b), F_1 increases up to more than 0.91, while the remaining fidelities are still small. This indicates a concentration of the population in the first manifold, and a state similar to a pure polariton. As P increases, $F_{n\pm}$ is non-zero for larger excitation numbers, but their values are very small. Changing the detuning, the fidelity of the steady state is always higher for the eigenstate with higher excitonic component; for negative detuning, higher fidelities are found for the upper polariton state.

So far we have only considered interaction between a single quantum dot and a cavity mode, but the model is valid for a system with many quantum dots in the case in which the quantum dots density is low enough to avoid direct interaction between excitons. Figure 12 shows linear entropy and negativity for the multiple quantum dots case as a function of the detuning between the exciton energy and the cavity mode when each quantum dot is being pumped at a rate $P = \kappa$. At this point, we focused exclusively in the set of parameters for which $\mathcal{N}$ is maximum for each number of QDs. As it can be seen, the detuning for maximum entanglement varies for each number of QDs, but the dependence of the negativity with the detuning does not change qualitatively. Low detunings are still not suitable to generate

N_ex	Δ/g	Eigenvalue	Eigenvector
1	0	0.270	$-0.704i\,\|G1\rangle + 0.711\,\|X0\rangle$
		0.262	$\|G0\rangle$
		0.253	$0.711\,\|G1\rangle - 0.704i\,\|X0\rangle$
	3	0.837	$-0.290\,\|G1\rangle + 0.957\,\|X0\rangle$
		0.080	$\|G0\rangle$
	20	0.995	$0.998\,\|X0\rangle - 0.050\,\|G1\rangle$
		0.002	$\|G0\rangle$

Table 1: Table of eigenvalues and eigenstates of the density matrix in the steady state for $\kappa = P$ and for different detunings. Three cases are considered: resonance, $\Delta \sim g$ and $\Delta \gg g$.

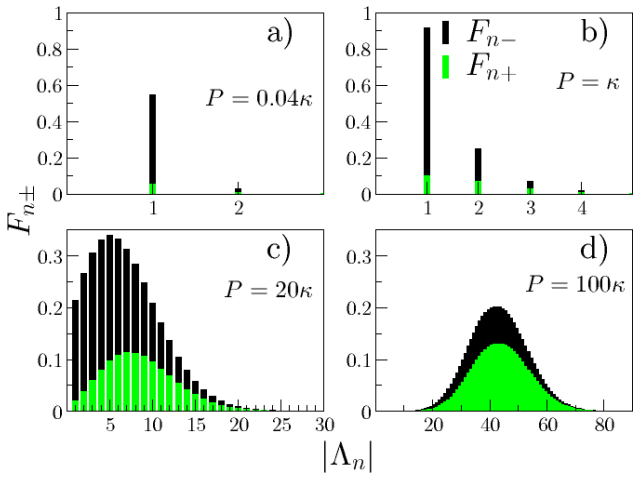

Figure 11: (Color online) Sequence of non-zero fidelities $F_{n\pm}$ between the steady state $\hat{\rho}_{ss}$ and the Λ_n–lower(black)/upper(green) polaritons $|n,\pm\rangle$ for $\kappa = 5 \times 10^{-3}$ meV, $\Delta = 3g$ and (a) $P = 0.04\kappa$, (b) $P = \kappa$, (c)$P = 20\kappa$ and (d) $P = 100\kappa$. $|\Lambda_n|$ denotes the excitation number of the polariton manifold Λ_n.

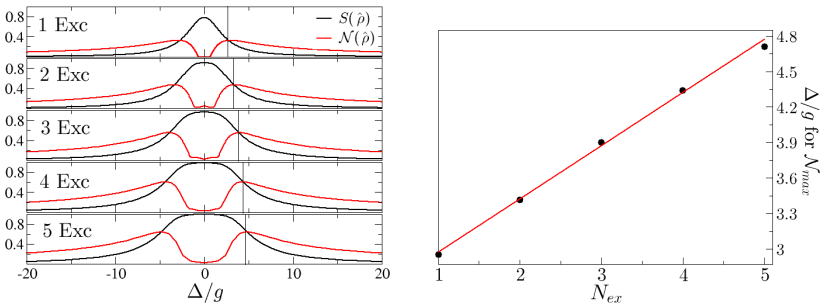

Figure 12: (Color online) Left: Negativity (red) and linear entropy (black) as a function of Δ for systems with different number of quantum dots (Exc). For all the cases, each QD interacts with the cavity mode with the same strength. Right: detuning for maximum entanglement as a function of the number of quantum dots.

non separable states because they maximize the degree of mixedness, and for large detunings, due to the absence of interaction, quantum dots saturate and hence the system is driven into a separable state. The competition between these two effects remains for systems with many non interacting QDs. While a direct comparison is not possible given that negativity has different maximum values for systems with Hilbert spaces of different size, the detuning for maximum entanglement in each specific number of QDs has been rigorously found. To verify that the general behavior does not change with the number of quantum dots, a diagonalization of the density operator is computed for the cases of 2 and 3 quantum dots. Results are displayed in table 2.

It shows that the case of many quantum dots does not differ qualitatively from the single quantum dot case, except for a shift of the detuning for which negativity is maximum in each case. Again, at resonance the state is an incoherent superposition of entangled and separable states, at large detunings the quantum dots saturate so the state is pure but separable and in the intermediate region the competition between mixedness and interaction drives the system into a non separable state.

2.3 QUANTUM DOT-QUANTUM DOT ENTANGLEMENT

A problem that naturally arises is whether or not the electromagnetic field is able to generate entanglement between two quantum dots. This is the most simple system able to present non local entanglement, a necessary condition for any quantum information protocol. To do so, a partial trace over the degree of freedom of the light is performed, and the negativity of the reduced operator of the QDs is calculated. This is

$$\hat{\rho}_{QD-QD} = \sum_{n} \langle n| \hat{\rho}_{ss} |n\rangle \tag{14}$$

Where $|n\rangle$ are the Fock states for the electromagnetic field and $\hat{\rho}_{ss}$ is the full density operator of the steady state. We perform this opera-

N_ex	Δ/g	Eigenvalue	Eigenvector
2	0	0.175	$-0.039i(\|XG1\rangle + \|GX1\rangle) - 0.576\|GG2\rangle + 0.816\|XX0\rangle$
		0.130	$0.707(\|XG0\rangle - \|GX0\rangle)$
		0.090	$0.707(\|XG1\rangle - \|GX1\rangle)$
	3	0.663	$-0.295(\|XG1\rangle + \|GX1\rangle) + 0.125\|GG2\rangle + 0.900\|XX0\rangle$
		0.125	$0.657(\|XG0\rangle + \|GX0\rangle) - 0.369\|GG1\rangle$
		0.108	$-0.356(\|XG2\rangle + \|GX2\rangle) + 0.172\|GG3\rangle + 0.846\|XX1\rangle$
	20	0.990	$-0.050(\|XG1\rangle + \|GX1\rangle) + 0.004\|GG2\rangle + 0.998\|XX0\rangle$
		0.005	$0.705(\|XG0\rangle + \|GX0\rangle)$
3	0	0.068	$-0.134(\|XGG2\rangle + \|GXG2\rangle + \|GGX2\rangle)$ $-0.276i(\|XXG1\rangle\|XGX1\rangle + \|GXX1\rangle) + 0.514i\|GGG3\rangle$
		0.061	$-0.110(\|XGG2\rangle + \|GXG2\rangle + \|GGX2\rangle)$ $+0.266i(\|XXG1\rangle + \|XGX1\rangle + \|GXX1\rangle) - 0.542i\|GGG3\rangle$
		0.053	$0.011i(\|XGG1\rangle + \|GXG1\rangle + \|GGX1\rangle)$ $-0.447(\|XXG0\rangle + \|XGX0\rangle + \|GXX0\rangle) + 0.633\|GGG2\rangle$
	4	0.664	$0.083(\|XGG2\rangle + \|GXG2\rangle + \|GGX2\rangle) - 0.034\|GGG3\rangle$ $-0.237(\|XXG1\rangle + \|XGX1\rangle + \|GXX1\rangle) + 0.900\|XXX0\rangle$
		0.119	$-0.243(\|XGG1\rangle + \|GXG1\rangle + \|GGX1\rangle)$ $+0.519(\|XXGO\rangle + \|XGX0\rangle + \|GXX0\rangle) + 0.116\|GGG2\rangle$
		0.112	$0.117(\|XGG3\rangle + \|GXG3\rangle + \|GGX3\rangle) - 0.052\|GGG4\rangle$ $-0.291(\|XXG2\rangle + \|XGX2\rangle + \|GXX2\rangle) + 0.838\|XXX1\rangle$
	20	0.985	$0.996\|XXX0\rangle - 0.050(\|XXG1\rangle + \|XGX1\rangle + \|GXX1\rangle)$

Table 2: Eigenvalues and eigenstates of the asymptotic density operator of the system for the cases of 2 and 3 quantum dots embedded in an optical microcavity. The quantum dots are in resonance between them and have a detuning Δ with the electromagnetic field. Again three cases are considered, resonance, detuning of the order of the interaction strength and large detuning.

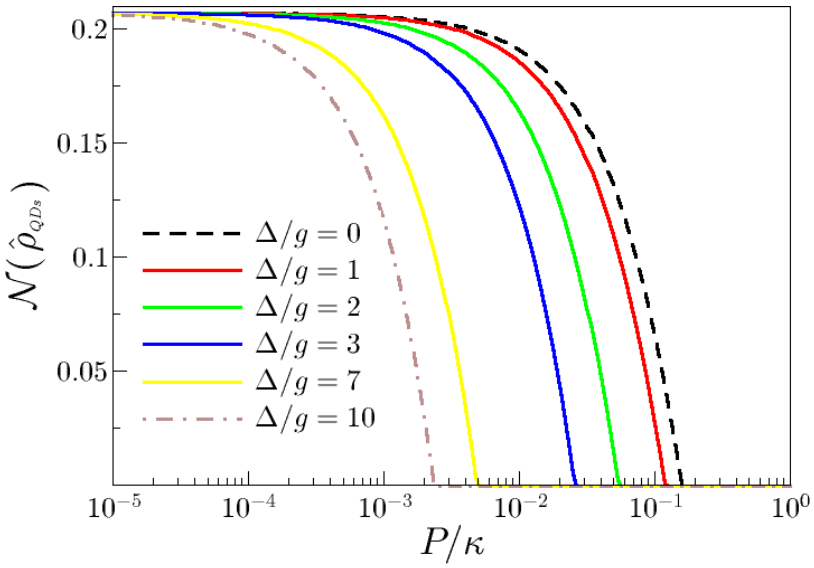

Figure 13: (Color online) Negativity of the reduced system of QDs in the steady state as a function of the incoherent pumping rate, for different values of the matter-light detuning. Contrary to the case of QD-light entanglement, resonance is the most suitable condition to find a non vanishing entanglement. In any case, the incoherent pumping has to be lower than the photon leakage rate.

tion for the case in which there are two quantum dots interacting with the cavity mode. Figure 13 shows the QD-QD entanglement quantified through negativity as a function of the pumping rate for different values of the light-matter detuning. In this case the condition $\kappa = P$ is not the most suitable anymore, in fact, there is a critical value of P for which the entanglement fully vanishes; this value is lower than the photon leakage rate. On the other hand, the figure also shows that the resonance condition enhances the QD-QD entanglement. Negativity is totally symmetric with respect to the sign of detuning, so, although figure 13 shows the results for positive detuning, they remain exactly the same for negative values.

2.4 CORRELATION PROPERTIES OF LIGHT

As mentioned in section 1.3, the correlation of the light emitted by the system has important information about the nature of the quasiparticles inside the cavity. Two quantities are computed with this aim, normalized second and third order correlation functions at $\tau = 0$. They are given by:

$$g^{(2)} = \frac{\langle \hat{a}^\dagger \hat{a}^\dagger \hat{a} \hat{a} \rangle}{\langle \hat{a}^\dagger \hat{a} \rangle^2} \tag{15}$$

$$g^{(3)} = \frac{\langle \hat{a}^\dagger \hat{a}^\dagger \hat{a}^\dagger \hat{a} \hat{a} \hat{a} \rangle}{\langle \hat{a}^\dagger \hat{a} \rangle^3} \tag{16}$$

Fig. 14 shows the dependence of the correlation functions with the incoherent pumping rate (left panel) and with the detuning (right

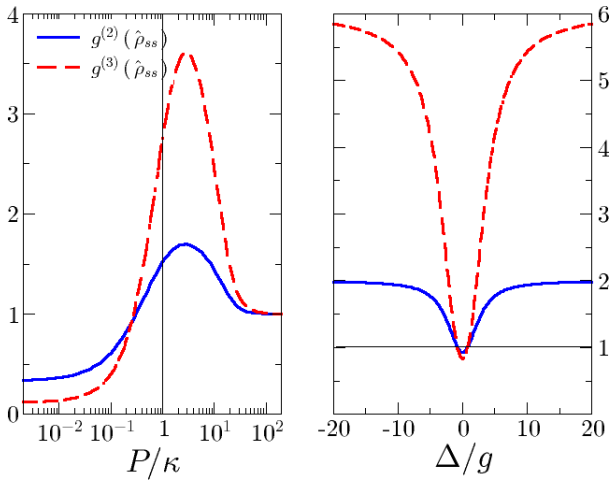

Figure 14: (Color online) Second (continuous blue) and third (dashed red) order correlation functions of the steady state of the system. The left panel shows the dependence with the incoherent pumping rate for the condition $\Delta = 3g$, while the right panel shows the dependence with Δ for the condition $P = \kappa$.

panel), for the single quantum dot case in the regimes of more interest: $\kappa = P$ and $\Delta = 3g$.

For small pumping power ($P < 0.2\kappa$) $g^{(2)}$, $g^{(3)} < 1$, a footprint of quantum light. As the pumping power increases both correlation functions grow monotonically, the light becomes chaotic $1 < g^{(2)} < 2$ and finally, for high pumping power the state of the field becomes coherent up to third order ($g^{(2)} = g^{(3)} = 1$), a condition that can be identified with a lasing regime.

On the other hand, by looking the dependence with the detuning (right panel of Fig. 14), near the resonance condition the state is almost second and third order coherent, so it can be again identified with a lasing regime. As the detuning increases $g^{(2)}$ and $g^{(3)}$ grow monotonically beyond 1, the emission of the system becomes chaotic. Finally, for large detuning, the cavity emission acquires thermal properties ($g^{(2)} = 2$).

2.5 OVERVIEW

In this work, we studied the properties of purity and entanglement of a microcavity-quantum dots system in the strong coupling regime by taking into account dissipative mechanisms, as well as the statistics of light in the case of interaction with a single emitter. For that case we also found the conditions for which the matter-light entanglement is maximized in the system. Matter and light should be out of resonance and incoherent pumping rate should exactly compensate the photon loss. This maximization is due to a competition of two effects: near resonance, the exchange of energy between the quantum dot and the cavity mode is enhanced, but the dissipation generates mixture in the steady state. In a large detuning condition, the degree of purity of

the steady state is enhanced, but the exchange of energy rate is not enough to generate non separable states. The value of Δ where these two effects compensate each other is around $\Delta \sim 3g$. Regarding to the pumping rate, the best condition is $P = \kappa$, the condition in which the exciton pumping exactly compensates the cavity losses.

In the case of many quantum dots, the best entanglement is reached when every quantum dot is pumped with a rate equal to the cavity losses. The most suitable condition is still $\Delta \neq 0$, although the exact value of the detuning slightly varies with the number of excitons. In this case the light is entangled with all the quantum dots, understood as one matter system.

Finally, we focused into the case of two quantum dots coupled through the cavity mode. We found that incoherent pumping strongly attempts against the coherence of the reduced matter system (QD-QD). The maximum QD-QD entanglement is obtained for an incoherent pumping at least one order of magnitude smaller than the photon leakage rate, in which case the system reaches an entanglement of 20%. The exciton energy should be also in resonance with the cavity mode, giving a criteria to identify two different regimes: if $\kappa = P$ and $\Delta \neq 0$ the system is in a state with light-matter quantum correlations, on the other hand, if the incoherent pumping is at least one order of magnitude below the dissipation rate, and the cavity mode has the same energy of the excitons, the system loses light-matter correlations, but the indirect interaction with the field drives the system in an entangled state of the quantum dots.

3

EFFECTS OF A COHERENT EXCITON PUMPING ON THE ENTANGLEMENT PROPERTIES OF POLARITONS IN MICROCAVITY - QUANTUM DOT SYSTEMS

A question that arises from chapter 2 is whether or not a non dissipative exciton pumping would drive the system into a more entangled steady state. In this chapter, we propose another mechanism to pump the system in order to reach a non trivial steady state. It consists in a coherent exciton pumping that compensates the photon leakage through cavity walls.

3.1 PHYSICAL SYSTEM AND THEORETICAL FRAME

The system under consideration is a single quantum dot (SQD) embedded in an optical microcavity (μC). The 3D confinement of the electron inside the dot produces a full quantization of its energy levels, and the confinement of light inside the μC allows to consider one single mode of the field[24], therefore, the full system can be described by a combination of direct products of a two level system ($|G\rangle, |X\rangle$) and a bosonic field ($|n\rangle$). Dipole interaction in the Strong Coupling (SC) regime can be considered as the most fundamental light-matter interaction mechanism in a $\mu C - SQD$ system and the Jaynes-Cummings model describes correctly the coherent exchange of energy between the emitter (QD) and the resonator mode[4]. The complete Hamiltonian, which takes into account matter-light interaction as well as the coherent exciton pumping is given by (in units $\hbar = 1$):

$$\begin{aligned}\hat{H} = \omega_o \hat{\sigma}^\dagger \hat{\sigma} + (\omega_o + \Delta)\hat{a}^\dagger \hat{a} + g(\hat{a}^\dagger \hat{\sigma} + \hat{a}\hat{\sigma}^\dagger) \\ + P_c(e^{i\omega_p t}\hat{\sigma}^\dagger + e^{-i\omega_p t}\hat{\sigma})\end{aligned} \tag{17}$$

Where ω_o is exciton's energy and Δ its difference with the energy of the electromagnetic field ($\omega_f = \omega_o + \Delta$), g is the light-matter interaction constant, P_c is the exciton coherent pumping rate, ω_p its frequency and t the time parameter. The operator $\hat{\sigma} = (\hat{\sigma}^\dagger)^\dagger = |G\rangle\langle X|$ is the fermionic annihilation operator for the SQD, while $\hat{a} = (a^\dagger)^\dagger$ is the usual annihilation operator for the cavity mode. Our model for the SQD in strong coupling with the cavity mode in presence of coherent exciton pumping and incoherent photon leakage through the cavity walls is sketched in figure 15.

Considering the Born-Markov approximation, the dynamics of the system are described by the master equation[33] (in units $\hbar = 1$):

$$\dot{\hat{\rho}} = i\left[\hat{\rho}, \hat{H}\right] + \hat{\mathcal{L}}(\kappa) \tag{18}$$

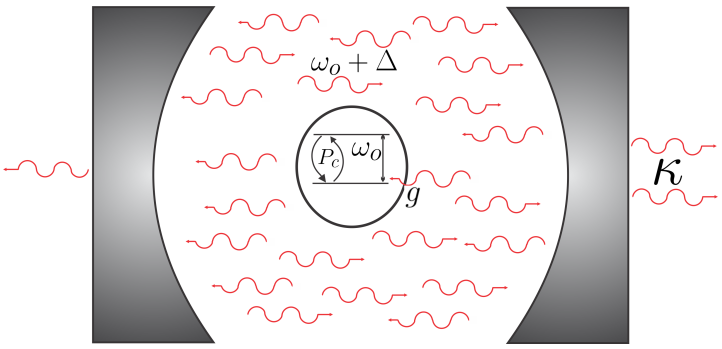

Figure 15: (Color online) Scheme of the SQD − μC system. The quantum dot sketched in the middle of the μC is in SC with the cavity mode (depicted in red) with coupling strength g. The SQD is also coherently pumped with rate P_c, and imperfections in the μC lead to photon scape at a rate κ.

In which the Liouville operator $\hat{\mathcal{L}}(\kappa) = \frac{\kappa}{2}(2\hat{a}\hat{\rho}\hat{a}^\dagger - \hat{a}^\dagger\hat{a}\hat{\rho} - \hat{\rho}\hat{a}^\dagger\hat{a})$ takes into account the incoherent loss of photons through the cavity walls.

To remove the dependence with time in the Hamiltonian, it is possible to change the representation picture by applying the unitary transformation[50] $\hat{\rho}' = \hat{U}^\dagger\hat{\rho}\hat{U}$. Where $\hat{U}$ is the unitary operator

$$\hat{U} = e^{-i((\omega_o-\Delta)\hat{a}^\dagger\hat{a}+\omega_o\hat{\sigma}^\dagger\hat{\sigma})} \tag{19}$$

A resonant pumping of the QD ($\omega_p = \omega_o$) eliminates emission lines from other QDs, reduces the cavity background emission and increases the vacuum Rabi splitting at $\Delta = 0$[18], a desirable condition when the interest is on a SQD. In this case, the dynamics of $\hat{\rho}'$ are described by the equation:

$$\dot{\hat{\rho}}' = i\left[\hat{\rho}', \hat{H}'\right] + \hat{\mathcal{L}}'(\kappa) \tag{20}$$

Where

$$\hat{H}' = \Delta\hat{a}^\dagger\hat{a} + g(\hat{a}^\dagger\hat{\sigma} + \hat{a}\hat{\sigma}^\dagger) + P_c(\hat{\sigma}^\dagger + \hat{\sigma}) \tag{21}$$

is the modified Hamiltonian and

$$\hat{\mathcal{L}}'(\kappa) = \frac{\kappa}{2}(2\hat{a}\hat{\rho}'\hat{a}^\dagger - \hat{a}^\dagger\hat{a}\hat{\rho}' - \hat{\rho}'\hat{a}^\dagger\hat{a}) \tag{22}$$

is the Liouville operator for the modified density matrix $\hat{\rho}'$.

3.2 DENSITY OPERATOR POPULATIONS

The principal interest is to study the properties of the polaritons inside the cavity for the steady state of the system ($\dot{\hat{\rho}}'(t)\to 0$), in order to identify the regimes in which they present a high degree of entanglement. To know which are the excitation manifolds with most probability it is necessary to study the diagonal terms (populations)

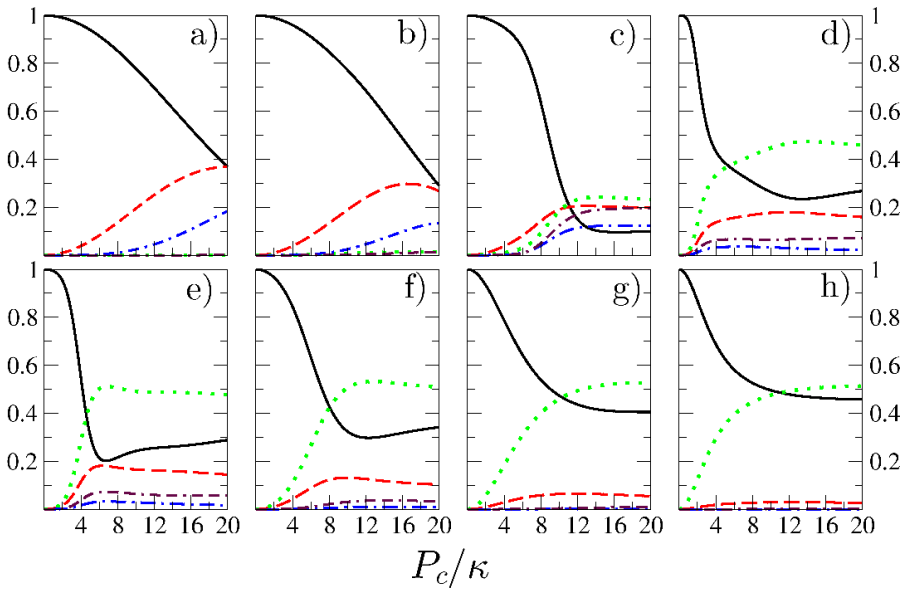

Figure 16: (Color online) Populations of $\hat{\rho}_{ss}$ as a function of the coherent pumping for different detunings: a)$\Delta = 0$, b)$\Delta = 0.02$ meV, c)$\Delta = 0.05$ meV, d)$\Delta = 0.1$ meV, e)$\Delta = 0.111$ meV, f)$\Delta = 0.15$ meV, g)$\Delta = 0.25$ meV and h)$\Delta = 0.4$ meV. The picture shows the population of the 3 first excitation manifolds: $\langle G0|\,\hat{\rho}_{ss}\,|G0\rangle$ (continuous black line), $\langle G1|\,\hat{\rho}_{ss}\,|G1\rangle$ (dashed red line), $\langle X0|\,\hat{\rho}_{ss}\,|X0\rangle$ (dotted green line), $\langle G2|\,\hat{\rho}_{ss}\,|G2\rangle$ (dashed-dotted blue line) and $\langle X1|\,\hat{\rho}_{ss}\,|X1\rangle$ (double dashed-dotted maroon line). For all the panels $g = 0.1$ meV, $\kappa = 5 \times 10^{-3}$ meV

of $\hat{\rho}_{ss}$ (density operator of the steady state), in this case, as a function of detuning between the bare modes (Δ) and exciton pumping rate (P_c). Results are displayed in figure 16.

In all the cases, populations are normalized to 1, so the figure shows that in the low pumping regime ($0 < P_c < g$) the population remains in the first three excitation manifolds for any detuning. Near the resonance (panels a) and b)) the QD remains in its ground state ($\langle X0|\,\hat{\rho}_{ss}\,|X0\rangle \to 0$ and $\langle X1|\,\hat{\rho}_{ss}\,|X1\rangle \to 0$), this suggests that the enhancement of the interaction due to the similar energies of exciton and photons makes the lifetime of the QD so low due to Purcell effect[51, 52] that the QD decays immediately after being excited by any mechanism (photon absorption or external matter pumping). Then, we do not expect polaritons near resonance to present entanglement. For larger detunings the decay time of the QD increases, so states $|X,0\rangle$ and $|X,1\rangle$ get populated (panels c) to f)). If we continue increasing the detuning there will not be light-matter interaction, the decay time of the QD will be much greater than the lifetime of a photon inside the microcavity so it will leak out of the cavity before being reabsorbed, then the system will not have photons in its steady state ($\langle G1|\,\hat{\rho}_{ss}\,|G1\rangle \to 0$ and $\langle X1|\,\hat{\rho}_{ss}\,|X1\rangle \to 0$), as it can be seen in panels

g) and h). The system will not be entangled in the steady state for large detunings neither. This gives a first glimpse of which are the regimes where the system could have a high degree of light-matter entanglement, the detuning has to be large enough so the exciton has a considerable lifetime, but low enough to not saturate the QD.

3.3 ENTANGLEMENT AND PURITY

A considerable probability of the states $|G1\rangle$ and $|X0\rangle$ is not enough to guarantee entangled polaritons (they could be in an incoherent superposition), the next step is then to compute the degree of entanglement and purity by using negativity and linear entropy, respectively (both normalized to 1). The former quantity is defined as the absolute value of the sum over all the negative eigenvalues of $\hat{\sigma}$, defined as a partial transpose of the density operator[25, 26] ($\sigma_{m\beta,n\alpha} = \rho_{m\alpha,n\beta}$). This quantity ranges from 0 to 1, and for this system, it is a witness of entanglement, instead of a quantifier. The latter quantity is defined as $S(\hat{\rho}) = 1 - \mathrm{Tr}[\hat{\rho}^2]$ which is 0 for a pure state and 1 for a maximally mixed state. Both quantities are strongly related, given that a high degree of entanglement requires a high degree of purity on the system[45, 48]. $\mathcal{N}$ and S are computed as a function of P_c and Δ, in order to find the sets of parameters in which the polaritons inside the cavity present strong quantum properties. Figure 17 shows negativity and linear entropy as a function of the coherent pumping for different detunings.

In resonance (panel a) the steady state of the system is pure ($S(\hat{\rho}_{ss}) = 0$), however, the intense interaction makes the quantum dot to decay very fast, the QD will decay as soon as an exciton is created, so the matter pumping will act more like a photon pumping, therefore the steady state of the system will have the form $|\psi\rangle = |G\rangle \otimes \sum_0^n a_i |i\rangle$, pure but separable. The coefficients a_i depend on the intensity of the matter pumping P_c
For large detunings matter and light decouple due to the absence of interaction, so the field will remain without photons, while matter will be in a (non coherent) superposition of its excited and ground states due to the pumping (panels g) and h)).
In the intermediate region $\frac{g}{2} \lesssim |\Delta| \lesssim 2g$ (panels b) to f)) there is a competition between these two mechanisms, and it is precisely there where polaritons present the most quantum properties: a high purity (low linear entropy) and considerable entanglement ($\mathcal{N} \gtrsim 0.3$). The maximum entanglement is found for $\Delta \approx 0.111$ meV and $P_c \approx 6\kappa \approx 0.03$ meV, and it has value of $\mathcal{N} \approx 0.36$.

Figure 18 shows the entanglement (continuous red line) and mixedness (dashed black line) of the steady state $\hat{\rho}_{ss}$ as a function of detun-

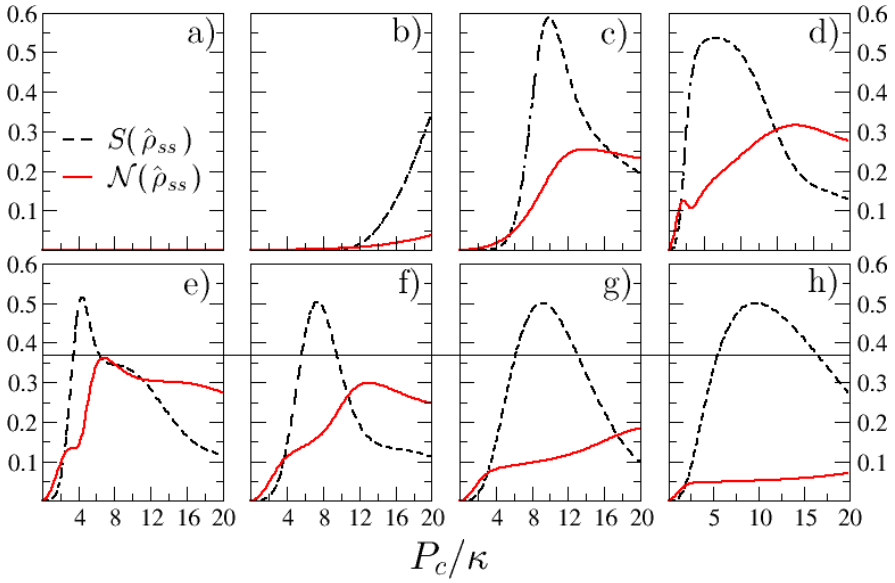

Figure 17: (Color online) Linear entropy (dashed black line) and negativity (continuous red line) of the system as a function of the coherent pumping rate P_c for a)$\Delta = 0$, b)$\Delta = 0.02$ meV, c)$\Delta = 0.05$ meV, d)$\Delta = 0.1$ meV, e)$\Delta = 0.111$ meV, f)$\Delta = 0.15$ meV, g)$\Delta = 0.25$ meV and h)$\Delta = 0.4$ meV. For all the panels $g = 0.1$ meV and $\kappa = 5 \times 10^{-3}$ meV

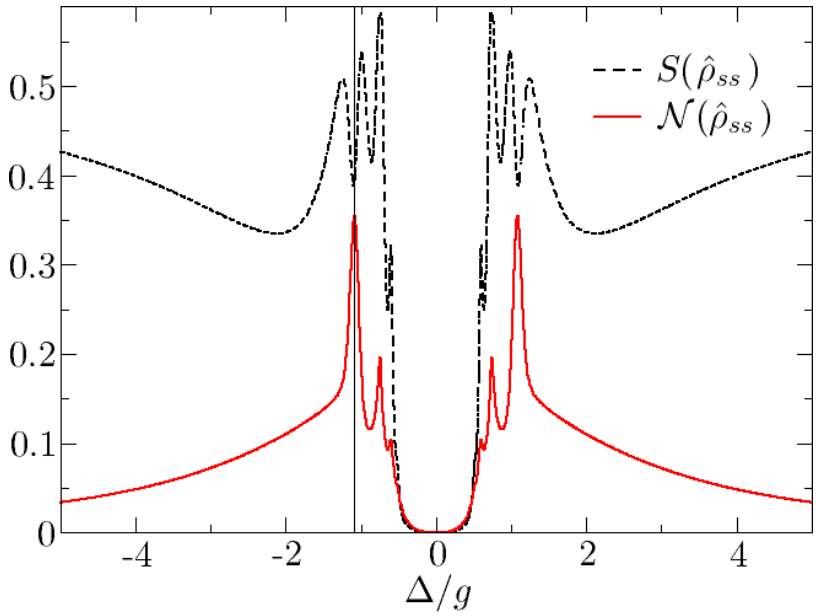

Figure 18: (Color online) Linear entropy (black dashed line) and negativity (red continuous line) of the steady state of the system for $g = 0.1$ meV, $\kappa = 5 \times 10^{-3}$ meV and $P_c = 0.0296$ meV as a function of the detuning Δ.

ing Δ. Notice that for $0 \lesssim |\Delta| \lesssim 0.3g$ the system is pure but not entangled. On the other hand, for $|\Delta| \gtrsim 2g$ the subsystems do not interact, so there is not entanglement in the steady state, the system is then in an incoherent superposition of the separable states $\frac{1}{\sqrt{2}}(|G\rangle + |X\rangle) \otimes |0\rangle$ and $\frac{1}{\sqrt{2}}(|G\rangle - |X\rangle) \otimes |0\rangle$ due to the coherent pumping and the incoherent loss of photons. It is then the competition between these mechanisms what generates a regime in which the subsystems get entangled, this is $0.3g \lesssim |\Delta| \lesssim 2g$. In this case, the interaction is strong enough to entangle the subsystems but not so high to make the decay time of the exciton lower than the lifetime of the photon inside the cavity. As a consequence, there is a minimum in the linear entropy of the state $(S(\rho_{ss})) \sim 0.38$ that coincides with a maximum in the entanglement ($\mathcal{N} \approx 0.36$), for $P_c \approx 0.3g = 0.03$ meV and $\Delta \approx 1.1g = 0.11$ meV.

3.4 DIAGONALIZATION OF $\hat{\rho}$ AND FIDELITY WITH A BELL STATE

For this system, negativity is not a direct measure of the entanglement degree, given that the light basis has more than 3 elements[26]. It is then helpful to study the state of the system in order to identify the degree of non-separability. The diagonalization of the density matrix $\hat{\rho}_{ss}$ can then give a glimpse in this direction. In the maximally entangled state achievable by the system, the system has a probability (eigenvalue) 0.75 of being in the pure entangled state:

$$\begin{aligned} |\psi\rangle &\approx (0.33 + 0.01i)\,|G,0\rangle + 0.80\,|X,0\rangle \\ &+ (0.47 - 0.01i)\,|G,1\rangle + (0.12 - 0.01i)\,|X,1\rangle + \dots \end{aligned} \tag{23}$$

Which is a considerably entangled system, given that $|X,0\rangle$ would have a probability of 0.65 while $|G,1\rangle$ would have probability of 0.22.
Competition between mixedness and coherent interaction generates a non trivial dependence of the calculated quantities, producing a full set of maxima and minima in the region in which no mechanism dominates as shown in figure 18.

To have a direct measure of how similar is $\hat{\rho}_{ss}$ to a Bell state we calculate its fidelity with a pure entangled polariton, understood as the eigenstate of the Jaynes-Cummings Hamiltonian:

$$H_{JC} = \Delta \hat{a}^\dagger \hat{a} + g(\hat{a}^\dagger \hat{\sigma} + \hat{a}\hat{\sigma}^\dagger) \tag{24}$$

At resonance, the corresponding eigenstates are precisely Bell states: maximally entangled states named "upper polariton state" ($|UP\rangle$) and "Lower polariton state" ($|LP\rangle$). In the first excitation manifold they are given by the expressions:

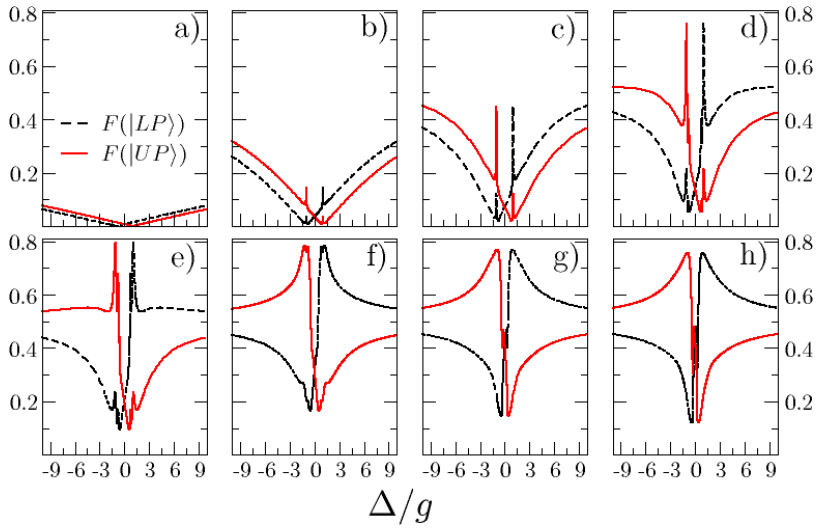

Figure 19: (Color online) Fidelity of the steady state of the system with a maximally entangled state of excitation manifold one, as a function of Δ for different pumping rates: a) $P_c = 0.001$ meV, b) $P_c = 0.005$ meV, c) $P_c = 0.01$ meV, d) $P_c = 0.02$ meV, e) $P_c = 0.0296$ meV, f) $P_c = 0.05$ meV, g) $P_c = 0.08$ meV and h) $P_c = 0.1$ meV. In all the cases $g = 0.1$ meV and $\kappa = 5 \times 10^{-3}$ meV.

$$|UP\rangle = \frac{1}{\sqrt{2}}(|X\rangle \otimes |0\rangle + |G\rangle \otimes |1\rangle) \tag{25}$$

$$|LP\rangle = \frac{1}{\sqrt{2}}(|X\rangle \otimes |0\rangle - |G\rangle \otimes |1\rangle) \tag{26}$$

The fidelity between a pure state $|\psi\rangle$ and a density operator $\hat{\rho}$ is defined as $F(|\psi\rangle) = \sqrt{\langle\psi|\,\hat{\rho}\,|\psi\rangle}$, it ranges from 0 (orthogonal states) to 1 (identical states)[49]. Fidelity between $\hat{\rho}_{ss}$ and the Bell states $|UP\rangle$ and $|LP\rangle$ is showed in figure 19 for different coherent pumping rates as a function of matter-light detuning Δ.
It shows that the system can have fidelities up to 0.8 with the lower or upper polariton, depending on the sign of the detuning. When exciton's energy is greater than light's ($\Delta < 0$), the system is in an upper polariton-like state (for $\Delta \sim -0.11$ meV), otherwise ($\Delta > 0$) it will be in a lower polariton-like state for $\Delta \sim 0.11$ meV.

3.5 OVERVIEW

We have computed the light-matter entanglement ($\mathcal{N}$) and linear entropy (S) for a microcavity - single quantum dot system in the steady state under a coherent excitonic pumping and an incoherent loss of photons through the cavity walls. We found a strong dependence of these quantum properties with the pumping rate and exciton-photon detuning. For small detunings Purcell effect enhances the emission of the dot, the exciton decays almost immediately after being created, so the pumping increases the number of photons inside the cavity while the quantum dot remains in its ground state.

On the other hand, for large detunings the quantum dot does not interact with the mode of the resonator, its decay times are much longer than the lifetime of a photon inside the cavity, so the probability of reabsorption vanishes. It is in a superposition of its ground and excited states (depending on the pumping rate) while the cavity has no photons.

Respecting to the pumping rate, low rates are not able to keep the dot excited in the steady state, while large pumping rates saturate the dot, attempting against its interaction with light. The system is separable in both cases.

The entanglement is greatly enhanced for $\Delta \sim g$ and $P_c \sim 6\kappa$. In this case, there is a competition between two mechanisms: matter-light interaction and incoherent loss of photons. In this regime, negativity reaches values up to 0.35 and linear entropy decreases up to 0.38. Since negativity does not quantify the degree of entanglement but works as a witness, a further analysis of the state is necessary. We computed the fidelity of the steady state of the system with a maximally entangled (Bell) state, and we found a fidelity greater than 80%, confirming that the state has a high degree of entanglement.

4

ENTANGLEMENT OF A SYSTEM OF 2 INTERACTING QD'S EMBEDDED IN AN OPTICAL MICROCAVITY. SOLUTION TO THE CLOSED PROBLEM IN THE FIRST EXCITATION MANIFOLD

As an extension of the problems addressed in chapters 2 and 3, in the present chapter we present a study the entanglement properties of a system of two interacting quantum dots embedded in an optical microcavity in the molecular regime, in which the strength of interaction between the quantum dots is higher than the interaction between the field and the quantum dots. Entanglement is quantified through the concurrence criteria. Since the aim is to study the entanglement by pairs, it is necessary to perform a partial trace over one of the three component systems and then calculate the concurrence of the remaining one. This is possible because the concurrence quantifies entanglement even for open systems[27].

4.1 MODEL AND THEORETICAL FRAMEWORK

Both quantum dots are treated as two level systems $|G_{1(2)}\rangle$ and $|X_{1(2)}\rangle$ (with energy transitions $\omega_1 = \omega_2 + \Delta$ and ω_2, respectively). They interact with each other through a dipolar-like term with parameter g_{12} and with the cavity mode $|n\rangle$ (whose energy is ω_C) via dipole interaction with strength g_1 and g_2, respectively. The term of interaction between the quantum dots can describe two different mechanisms: a resonant energy transfer known as Förster interaction[40, 53] or a tunneling of the electron from one quantum dot to another, forming the so called "indirect exciton"[41]. The values of the parameters employed are typical in experiments in which the second mechanism dominates the energy transfer between quantum dots[39]. The Hamiltonian of the system is then (in units $\hbar = 1$):

$$\begin{aligned} H = \omega_C \hat{a}^\dagger \hat{a} + (\omega_2 + \Delta)\hat{\sigma}_1^\dagger \hat{\sigma}_1 + \omega_2 \hat{\sigma}_2^\dagger \hat{\sigma}_2 + g_1(\hat{a}\hat{\sigma}_1^\dagger + \hat{a}^\dagger \hat{\sigma}_1) \\ + g_2(\hat{a}\hat{\sigma}_2^\dagger + \hat{a}^\dagger \hat{\sigma}_2) + g_{12}(\hat{\sigma}_1 \hat{\sigma}_2^\dagger + \hat{\sigma}_1^\dagger \hat{\sigma}_2) \end{aligned} \tag{27}$$

Where $\hat{a} = (\hat{a}^\dagger)^\dagger$ is the annihilation operator for the electromagnetic field, and $\hat{\sigma}_i = (\hat{\sigma}_i^\dagger)^\dagger = |G_i\rangle \langle X_i|$ is the annihilation operator for each quantum dot. As a first approach we study the closed case, in which the number of excitations (which is a preserved quantity of the system, given that $\hat{H}$ commutes with $\hat{N}$) is 1. We distinguish four conditions of interest given by a tune of the electromagnetic field's energy. They are evidenced in the diagrams of eigenenergies as a function of the detuning between the quantum dots Δ:

1. The first case of interest is an anticrossing of the cavity mode's energy with the lower branch. Given that there is a direct dipole interaction it is enough to tune the field (ω_C) in an energy below ω_2.

2. There is a special case in which, despite the term of dipole interaction, the system presents a crossing with the lower branch. The energy of the field in this case is

$$\omega_C = \frac{\omega_1 + \omega_2}{2} - \frac{g_{12}}{2}\left[\frac{g_1}{g_2} + \frac{g_2}{g_1}\right] + \frac{g_1 g_2}{g_{12}}$$

   This value was theoretically calculated by the exact diagonalization of $\hat{H}$. It corresponds to the only case in which there is a degeneration in the energies of the system. The complete calculation is showed in Appendix B (chapter 7).

3. The third case is a maximization of the anticrossing with the upper branch. To reach this condition ω_C should be given by

$$\omega_C = \frac{\omega_1 + \omega_2}{2} + \frac{1}{2} g_{12}\left[\frac{g_1}{g_2} + \frac{g_2}{g_1}\right]$$

   It has been also exactly calculated by maximizing the difference between two eigenenergies of the system. Its complete calculation is also showed in Appendix B (chapter 7).

4. The last studied case is a regular anticrossing condition with the upper branch. To reach this situation it is enough to tune the field's energy beyond ω_2.

We quantify the entanglement between pairs of subsystems by calculating their reduced density operator, this is the state obtained after perform a partial trace over the degrees of freedom in which we are not interested. In general, the reduced operator is not pure, and it is given by (for a system of three qubits):

$$\hat{\rho}_{12} = \langle 0_3|\hat{\rho}|0_3\rangle + \langle 1_3|\hat{\rho}|1_3\rangle \tag{28}$$

Where $\hat{\rho}$ is the density operator of the full system and $|0_3\rangle$ and $|1_3\rangle$ are the two accessible levels of the system over which the partial trace is being performed. The degree of entanglement is calculated through concurrence [27], defined in equations 4 and 5.

4.2 ENTANGLEMENT OF THE EIGENSTATES

Unless stated different, the energy of the second quantum dot is fixed at $\omega_2 = 1$ eV, and given that the interest lies in the molecular regime in which the interaction between the quantum dots is higher than the interaction of each quantum dot with the field, we set $g_{12} = 1$ meV, $g_1 = 0.1$ meV and $g_2 = 0.03$ meV. For the first case, the diagonalization of the Hamiltonian together with the concurrence of the system

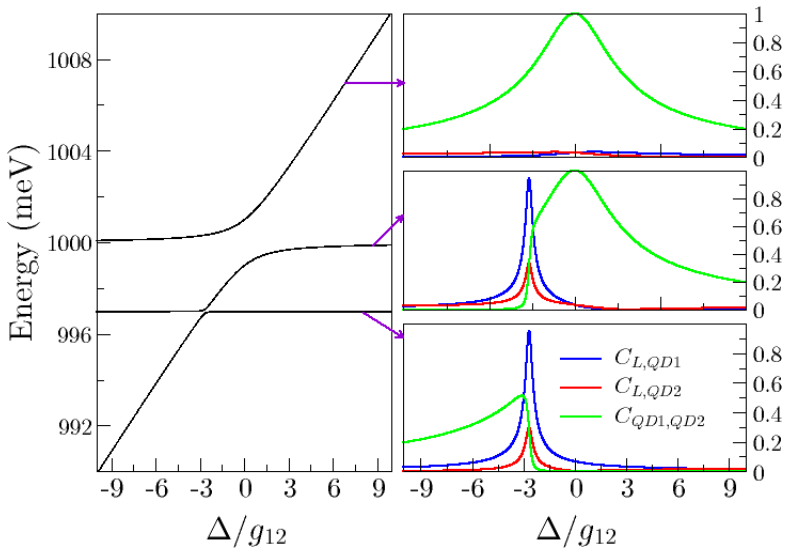

Figure 20: (Color online) Eigenstates of the system and entanglement by pairs measured by concurrence for each branch of the dispersion diagram for the case in which the light anticrosses the lower branch of the QD molecule ($\omega_C = 997$ meV). The blue line shows the concurrence of the reduced system light-quantum dot 1, the red one shows the concurrence of the system Light-Quantum dot 2, and the green line shows the entanglement between the quantum dots.

are showed in figure 20. Notice for the lower branch, that the anticrossing coincides with a maximum entanglement between light and QD1, due to direct interaction through the parameter g_1, however, at this point there is also a maximum entanglement between the second QD and the light; this is expected because the interaction between them is enhanced by the first QD, which interact strongly with both of them; they get entangled by their indirect interaction through the first QD.
For high Δ (positive and negative) we have the separable state $|1XG\rangle$ (upper and lower branch, respectively) and an entangled state between light and QD2. The value of this entanglement depends on the difference of energies between the field and the QD2 (neither of them depends on Δ). Finally, for the second and third branches there is a value of the detuning in which light and QD2 totally decouple (in $\Delta/g_{12} \approx -2.3$). The origin of this special value is not clear yet, given that in the dispersion diagram this point has not any special condition.

The next condition we are interested in, is the crossing condition, for which the dispersion diagram and the entanglement are showed in figure 21. In this case, the band diagram looks like the one of two interacting quantum dots with a non-interacting field, however, the concurrence between the field and the second dot is not 0, independently of the energy ω_2, which means that the subsystems are coupled despite the crossing. By looking the horizontal branch it is pos-

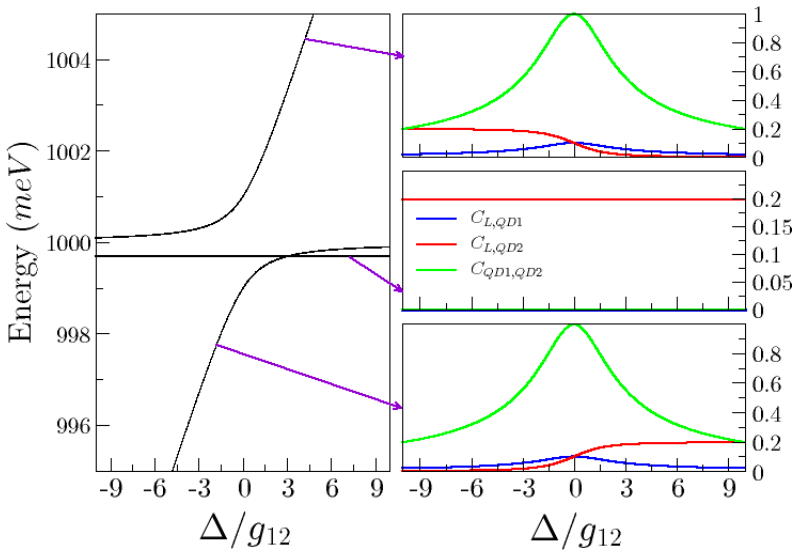

Figure 21: (Color online) Eigenstates of the system and entanglement by pairs (concurrence) for each branch of the dispersion diagram for the condition of crossing ($\omega_C = 999.703$ meV). There are two branches that anticross as expected in a typical QD-QD interaction problem, and a third branch that crosses the lower one, corresponding to a state with small entanglement between the cavity and the second quantum dot.

sible to notice that its energy is not exactly the one of the field, it is a polaritonic state conformed by the light and a little contribution of the second QD.
Again, for large detunings the system can be in a polaritonic state composed by the second QD and light, and in the separable state $|0XG\rangle$.

Another interesting case is the one for which the anticrossing is maximum. Its dispersion diagram together with the concurrence of their constituent systems are shown in figure 22. Again, for the two lower branches there are special points in which the light and the second QD get disentangled, however, in the dispersion diagram these points do not look like special points, for example, in the concurrence for the middle branch, the entanglement between light and second quantum dot is 0 for $\Delta/g_{12} \approx 8$, but the systems are still interacting (ω_2, ω_f and g_2 do not change with Δ).

Finally, we study the case in which the light branch anticrosses the upper branch. The energies and the entanglement are shown in figure 23. Again, in the middle branch, there is a particular value of the detuning for which the entanglement between light and QD2 goes to 0, since the interaction parameters between them do not depend of the detuning, we conclude that the energy of the first QD affects critically the entanglement between the second QD and the mode of the cavity, this is not evident from the dispersion diagram, though.

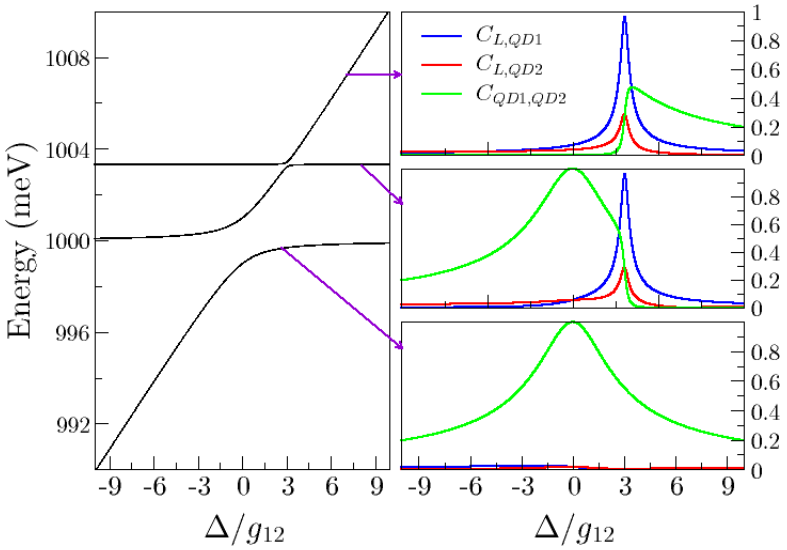

Figure 22: (Color online) Eigenstates of the system and concurrences for each branch of the dispersion diagram in the condition of maximum anticrossing with the upper branch ($\omega_C = 1003.33$ meV).

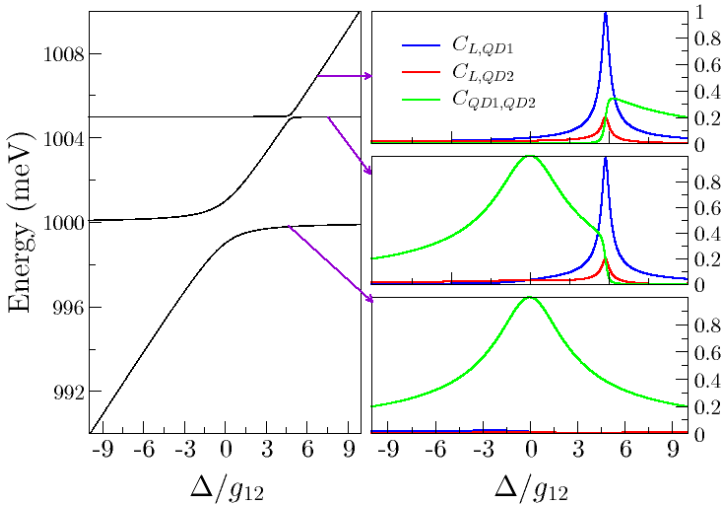

Figure 23: (Color online) Eigenstates of the system and entanglement by pairs for each branch of the dispersion diagram in the condition of regular anticrossing with the upper branch ($\omega_C = 1005$ meV).

4.3 OVERVIEW

In the present work we have studied the entanglement properties of a system of two interacting quantum dots embedded in an optical microcavity. As a first approach to a more complete problem we studied the Hamiltonian case in which dissipative effects are small enough to be neglected. The interest lay in the entanglement of the eigenstates of $\hat{H}$ quantified through the concurrence defined in eqs. 4 and 5.

A remarkable case is the one in which the field's branch crosses the lower branch of the molecular system. This eigenstate corresponds to a total decoupling between the quantum dots, and between the light and the first quantum dot, but there is a remaining entanglement between the light and the second quantum dot. In the other three studied cases the entanglement between the quantum dots is favored, given that their interaction strength is larger than the dipole interaction, as evidenced by the green lines in figures 20, 22 and 23. When the cavity mode and the first quantum dot are in resonance their interaction is enhanced and the entanglement between quantum dots is replaced by light-matter entanglement (blue lines). In this case, there is also a maximum in the entanglement between the second quantum dot and the field, given that, besides the direct interaction with strength g_2, they are interacting indirectly through the first quantum dot, which interact strongly with each of them.

Part III

CONCLUSIONS AND APPENDICES

5

CONCLUSIONS AND PERSPECTIVES

In this thesis three theoretical works on quantum dot-microcavity systems have been presented. The main results of each work can be summarized as follows:

In chapter 2 we studied the properties of purity and entanglement of a microcavity-quantum dots system in the strong coupling regime by taking into account two dissipative mechanisms: photon leakage through cavity walls and exciton pumping. In the case of a single quantum dot we found the conditions for which the matter-light entanglement is maximized in the system. Matter an light should be out of resonance and incoherent pumping rate should exactly compensate the photon loss. This maximization is due to a competition of two effects: near resonance, the exchange of energy between the quantum dot and the cavity mode is enhanced, but the dissipation generates mixture in the steady state. In a large detuning condition, the degree of purity of the steady state is enhanced, but the exchange of energy rate is not enough to generate non separable states. The value of Δ where these two effects compensate each other is around $\Delta \sim 3g$. Regarding to the pumping rate, the best condition is $P = \kappa$, the condition in which the exciton pumping exactly compensates the cavity losses.
In the case of many quantum dots, the best entanglement is reached when every quantum dot is pumped with a rate equal to the cavity losses. The most suitable condition is still $\Delta \neq 0$ although the exact value of the detuning slightly varies with the number of excitons. In this case the light is entangled with all the quantum dots, understood as one matter system.
Finally, we focused into the case of two quantum dots coupled through the cavity mode. We found that incoherent pumping strongly attempts against the coherence of the reduced matter system (QD-QD). The maximum QD-QD entanglement is obtained for an incoherent pumping at least one order of magnitude smaller than the photon leakage rate, in which case the system reaches an entanglement of 20%. The exciton energy should be also in resonance with the cavity mode, giving a criteria to identify two different regimes: if $\kappa = P$ and $\Delta \neq 0$ the system is in a state with light-matter quantum correlations, on the other hand if the incoherent pumping is at least one order of magnitude below the dissipation rate, and the cavity mode has the same energy of the excitons, the system loses light-matter correlations, but the indirect interaction with the field drives the system in an entangled state of the quantum dots.

In chapter 3 we have computed the light-matter entanglement ($\mathcal{N}$) and linear entropy (S) for a microcavity - single quantum dot system

in the steady state under a coherent excitonic pumping and an incoherent loss of photons through the cavity walls. We found a strong dependence of these quantum properties with the pumping rate and exciton-photon detuning. For small detunings Purcell effect enhances the emission of the dot, the exciton decays almost immediately after being created, so the pumping increases the number of photons inside the cavity while the quantum dot remains in its ground state.
On the other hand, for large detunings the quantum dot does not interact with the mode of the resonator, its decay times are much longer than the lifetime of a photon inside the cavity, so the probability of reabsorption vanishes. It is in a superposition of its ground and excited states (depending on the pumping rate) while the cavity has no photons.

Respecting to the pumping rate, low rates are not able to keep the dot excited in the steady state, while large pumping rates saturate the dot, attempting against its interaction with light. The system is separable in both cases. The entanglement is greatly enhanced for $\Delta \sim g$ and $P_c \sim 6\kappa$. In this case, there is a competition between two mechanisms: matter-light interaction and incoherent loss of photons. In this regime, negativity reaches values up to 0.35 and linear entropy decreases up to 0.38. Since negativity does not quantify the degree of entanglement but works as a witness, a further analysis of the state is necessary. We computed the fidelity of the steady state of the system with a maximally entangled (Bell) state, and we found a fidelity greater than 80%, confirming that the state has a high degree of entanglement.

Finally, in chapter 4 we made a first approach to the problem in which the density of quantum dots is high enough so they are able to interact either via Förster interaction or by electron tunneling, when dissipative effects are low enough to be neglected. In this case we used the typical parameters of the second mechanism. We focused in the molecular case, when the interaction between quantum dots is higher than dipolar interaction with the cavity mode. The goal was to study the entanglement of the eigenstates of the hamiltonian, quantified by using the concurrence criteria. Four cases were considered, a regular anticrossing with the lower branch, a crossing, a maximization of the anticrossing and a regular anticrossing with the upper branch. In each case, a characterization of the entanglement by pairs of the eigenstates associated with each of the three branches was performed.

A natural perspective is the design of experiments to measure the degree of light-matter entanglement inside a microcavity with quantum dots embedded, in order to validate the theoretical predictions made by quantum mechanics. On the other hand, given that the most suitable state to perform quantum information processing operations is the Bell state, it worths to keep looking for mechanisms able to protect the stationary entanglement from dissipation.

6

APPENDIX A: DETAILS ON THE SOLUTION OF THE MASTER EQUATION

In this appendix, we will discuss the obtainment and diagonalization of the density matrix $\hat{\rho}$ for the problems addressed in chapters 2 and 3. To solve the dynamics of the system and its steady state by using the master equations 13 and 18 (in chapters 2 and 3, respectively), it is mandatory to pick a basis to expand the operator, in order to obtain the system of differential equations corresponding to each term of $\hat{\rho}$. In this case, a good choice is the bare states basis, conformed by the direct products of the matter states $|G\rangle$ and $|X\rangle$, and the bosonic states of the cavity mode $|n\rangle$. It is important to take into account that the excitation manifold is not a preserved quantity; the dissipative processes and the coherent matter pumping, break this symmetry in such a way, that the population can reach states with any number of excitations, given that, in theory, the cavity mode has infinite accessible states. Figure 24 depicts the ladder of states for the system and the way that photon leakage and exciton pumping (coherent and incoherent) lead the system between states of different excitation manifold.

This symmetry rupture, makes necessary to perform a truncation in the basis, in order to be able to solve numerically the problem. The criteria to truncate, is the convergence to 0 of the terms corresponding to the most excited states. Each term of the density matrix corresponds to the scalar product of two vectors, and for each state of the basis there is a corresponding number. For example, if we assign the label i to the state $|M, n\rangle$ and the label j to $|M', n'\rangle$, the component i, j of the density matrix expanded in the chosen basis would be given by:

$$\rho_{i,j} = \langle M, n| \hat{\rho} |M', n'\rangle \tag{29}$$

This is the way how the operator is numerically treated. In the steady state, the density operator does not change in time, this means $\dot{\hat{\rho}} \to 0$. As a consequence, the system of differential equations is reduced to a linear system when expanded in the chosen basis. This system is numerically solved. All the information we can obtain about the system is contained in the density operator.

Once we have obtained $\hat{\rho}_{ss}$, the calculation of the desired quantities is made by performing different operations on it, such as partial transpose, multiplications by matrices or vectors, etc. The diagonalization, made in order to get tables 1 and 2, is also numerically obtained, given the high dimensions of the basis. The interpretation is as follows: each eigenvalue is the probability that the system has, of being in the pure state corresponding to its eigenvector. The great

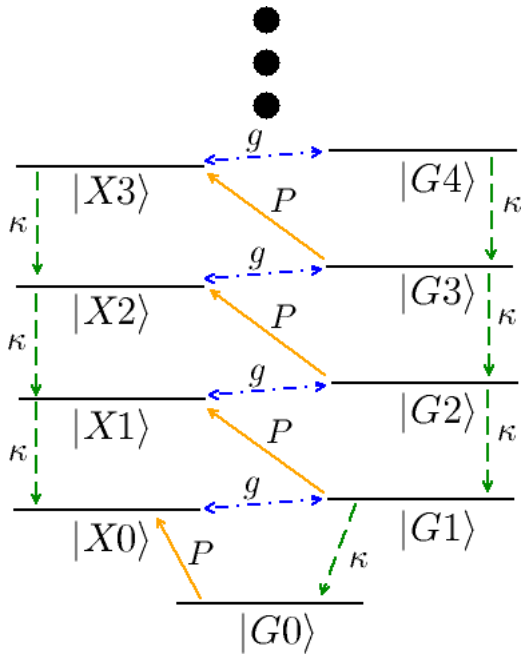

Figure 24: Ladder of states for the Jaynes-Cummings model by excitation manifolds. The figure includes photon leakage through cavity walls (dashed-dotted green arrows) and exciton pumping (coherent or incoherent; continuous orange arrows). Dashed-dotted blue lines represent the coherent exchange of energy (dipole interaction). Notice that this is the only mechanism that generates transitions between states of the same manifold.

difference of this probability, with the probability associated to the coefficients of each pure state, is in the coherence; an interference experiment would distinguish a coherent (pure) superposition from an incoherent one i.e. the one associated with the diagonalization of $\hat{\rho}$.

7

APPENDIX B: SPECIAL VALUES OF ω_C FOR THE PROBLEM OF TWO INTERACTING QUANTUM DOTS

We show the calculations made in order to obtain the values of ω_C for the crossing with the lower branch and for the maximization of the anticrossing with the upper one. In both cases, the hamiltonian of the system is given by (in units $\hbar = 1$):

$$\hat{H} = \omega_C \hat{a}^\dagger \hat{a} + (\omega_2 + \Delta)\hat{\sigma}_1^\dagger \hat{\sigma}_1 + \omega_2 \hat{\sigma}_2^\dagger \hat{\sigma}_2 + g_1(\hat{a}\hat{\sigma}_1^\dagger + \hat{a}^\dagger \hat{\sigma}_1) + g_2(\hat{a}\hat{\sigma}_2^\dagger + \hat{a}^\dagger \hat{\sigma}_2) + g_{12}(\hat{\sigma}_1 \hat{\sigma}_2^\dagger + \hat{\sigma}_1^\dagger \hat{\sigma}_2) \quad (30)$$

The complete basis for the problem is the direct product of the accessible states for each quantum dot ($|G_{1(2)}\rangle$ and $|X_{1(2)}\rangle$) and the bosonic light field up to first excitation manifold ($|0\rangle$ and $|1\rangle$), however a rotation of the matter states will be convenient, so we choose the basis resulting from the solution to the problem of two interacting quantum dots in the absence of radiation, for which the hamiltonian is:

$$\hat{H}_{QDs} = (\omega_2 + \Delta)\hat{\sigma}_1^\dagger \hat{\sigma}_1 + \omega_2 \hat{\sigma}_2^\dagger \hat{\sigma}_2 + g_{12}(\hat{\sigma}_1 \hat{\sigma}_2^\dagger + \hat{\sigma}_1^\dagger \hat{\sigma}_2) \quad (31)$$

For this system, the eigenstates are:

$$|\psi_1\rangle = Cos(\theta)|XG\rangle + Sin(\theta)|GX\rangle \quad (32)$$

$$|\psi_2\rangle = -Sin(\theta)|XG\rangle + Cos(\theta)|GX\rangle \quad (33)$$

Where θ is given by:

$$Tan(\theta) = \frac{g_{12}}{\frac{\Delta}{2} + \sqrt{g_{12}^2 + \frac{\Delta^2}{4}}} \quad (34)$$

If we write the matrix form of the hamiltonian 30 in this new basis, organized as follows: $\{|1, G, G\rangle, |0, \psi_1\rangle, |0, \psi_2\rangle\}$ (notice that the three vectors are orthogonal in a space of dimension 3, hence, they form a basis), it has the form:

$$\begin{pmatrix} \widetilde{\omega_C} & g_1 Cos(\theta) + g_2 Sin(\theta) & -g_1 Sin(\theta) + g_2 Cos(\theta) \\ g_1 Cos(\theta) + g_2 Sin(\theta) & \sqrt{g_{12}^2 + \frac{\Delta^2}{4}} & 0 \\ -g_1 Sin(\theta) + g_2 Cos(\theta) & 0 & -\sqrt{g_{12}^2 + \frac{\Delta^2}{4}} \end{pmatrix}$$

Where

$$\widetilde{\omega_C} = \omega_C - \frac{\omega_1 + \omega_2}{2} \quad (35)$$

If we define two new quantities: $g_u = g_1 Cos(\theta) + g_2 Sin(\theta)$ and $g_l = -g_1 Sin(\theta) + g_2 Cos(\theta)$ we can write $\hat{H}$ as follows:

$$\begin{pmatrix} \widetilde{\omega_C} & g_u & g_l \\ g_u & \sqrt{g_{12}^2 + \frac{\Delta^2}{4}} & 0 \\ g_l & 0 & -\sqrt{g_{12}^2 + \frac{\Delta^2}{4}} \end{pmatrix}$$

This redefinition gives us a new interpretation of the problem. Now we can see g_u and g_l as effective coupling constants. Since the interest is to find a crossing and a maximum anticrossing, we should maximize g_u with the parameter θ. From where we obtain $Sin(\theta) = Cos(\theta)\frac{g_2}{g_1}$. This condition implies that g_l vanishes, and that detuning between the quantum dots can be related with the coupling constants as (by replacing $Tan(\theta)$ in 34):

$$\Delta = g_{12}\left(\frac{g_1}{g_2} - \frac{g_2}{g_1}\right) \tag{36}$$

And replacing in g_u and g_l we obtain:

$$g_u = \sqrt{g_1^2 + g_2^2} \tag{37}$$

$$g_l = 0 \tag{38}$$

Rewriting $\hat{H}$ for this new condition we obtain:

$$\begin{pmatrix} \widetilde{\omega_C} & \sqrt{g_1^2 + g_2^2} & 0 \\ \sqrt{g_1^2 + g_2^2} & \sqrt{g_{12}^2 + \frac{\Delta^2}{4}} & 0 \\ 0 & 0 & -\sqrt{g_{12}^2 + \frac{\Delta^2}{4}} \end{pmatrix}$$

The eigenvalues for this new matrix i.e. the eigenenergies of the system, in descendant order are given by:

$$E_1 = \frac{1}{2}\left(\widetilde{\omega_C} + \sqrt{g_{12}^2 + \frac{\Delta^2}{4}}\right) + \frac{1}{2}\sqrt{\left(\widetilde{\omega_C} - \sqrt{g_{12}^2 + \frac{\Delta^2}{4}}\right)^2 + 4(g_1^2 + g_2^2)} \tag{39}$$

$$E_2 = \frac{1}{2}\left(\widetilde{\omega_C} + \sqrt{g_{12}^2 + \frac{\Delta^2}{4}}\right) - \frac{1}{2}\sqrt{\left(\widetilde{\omega_C} - \sqrt{g_{12}^2 + \frac{\Delta^2}{4}}\right)^2 + 4(g_1^2 + g_2^2)} \tag{40}$$

$$E_3 = -\sqrt{g_{12}^2 + \frac{\Delta^2}{4}} \tag{41}$$

At this point we are ready to find the energies of the cavity mode that generate crossing and maximum anticrossing, respectively. For the first case it is enough to make $E_2 = E_3$ and find ω_C, from where we obtain:

$$\omega_C = \frac{\omega_1 + \omega_2}{2} - \frac{1}{2}g_{12}\left(\frac{g_1}{g_2} + \frac{g_2}{g_1}\right) + \frac{g_1 g_2}{g_{12}} \tag{42}$$

For the anticrossing condition we make a comparison with the Jaynes - Cummings energies $\omega_C \pm \sqrt{\delta^2 + 4g^2}$. If we associate the term $\widetilde{\omega_C} - \sqrt{g_{12}^2 + \frac{\Delta^2}{4}}$ in E_1 and E_2, with δ, the resonance condition ($\delta = 0$) is given by (replacing Δ from eq. 36):

$$\omega_C = \frac{\omega_1 + \omega_2}{2} + \frac{1}{2}g_{12}\left(\frac{g_1}{g_2} + \frac{g_2}{g_1}\right) \tag{43}$$

BIBLIOGRAPHY

[1] Anonymous. Proceedings of the American Physical Society. *Phys. Rev.*, 69:674–674, Jun 1946.

[2] Fabrice P. Laussy, Elena del Valle, and Carlos Tejedor. Luminescence spectra of quantum dots in microcavities. I. Bosons . *Phys. Rev. B*, 79(235325), Jun 2009.

[3] E. T. Jaynes and F. W. Cummings. Comparison of quantum and semiclassical radiation theories with application to the beam maser. *Proc. IEEE*, 51(89), Jan 1963.

[4] Bruce W. Shore and Peter L. Knight. The Jaynes-Cummings model. *Journal of Modern Optics*, 40(7):1195–1238, Jan 1993.

[5] M. Brune, F. Schmidt-Kaler, A. Maali, J. Dreyer, E. Hagley, J. M. Raimond, and S. Haroche. Quantum Rabi Oscillation: A Direct Test of Field Quantization in a Cavity. *Phys. Rev. Lett.*, 76:1800–1803, Mar 1996.

[6] Wallraff A., Schuster D. I., Blais A., Frunzio L., Huang R.- S., Majer J., Kumar S., Girvin S. M., and Schoelkopf R. J. Strong coupling of a single photon to a superconducting qubit using circuit quantum electrodynamics. *Nature*, 431(7005):162–167, Sep 2004.

[7] J. P. Reithmaier, G. Sek, A. Loffler, C. Hofmann, S. Kuhn, S. Reitzenstein, L. V. Keldysh, V. D. Kulakovskii, T. L. Reinecke, and A. Forchel. Strong coupling in a single quantum dot–semiconductor microcavity system . *Letters to Nature*, 432, Nov 2004.

[8] C. Weisbuch, M. Nishioka, A. Ishikawa, and Y. Arakawa. Observation of the coupled exciton-photon mode splitting in a semiconductor quantum microcavity. *Phys. Rev. Lett.*, 69:3314–3317, Dec 1992.

[9] Iulia Buluta, Sahel Ashhab, and Franco Nori. Natural and artificial atoms for quantum computation. *Reports on Progress in Physics*, 74(10):104401, Sep 2011.

[10] J. Vučković, D. Englund, A. Faraon, I. Fushman, and E. Waks. *Quantum Information Processing with Quantum Dots in Photonic Crystals*. Pan Stanford Publishing, 2008.

[11] Khitrova G., Gibbs H. M., Kira M., Koch S. W., and Scherer A. Vacuum Rabi splitting in semiconductors. *Nat Phys*, 2(2):81–90, Feb 2006.

[12] Randolf W. Knoss. *Quantum dots: research, technology and applications*. Nova Science Publishers, Inc., 2009.

[13] Peter A. Ling. *Quantum dots: new research*. Nova Science Publishers, Inc., 2005.

[14] K. J. Vahala. Optical microcavities. *Nature*, 424, Aug 2003.

[15] J. L. Vossen and W. Kern. *Thin film processes*. Academic Press, 1978.

[16] B. A. Joyce. Molecular beam epitaxy. *Reports on progress in Physics*, 48(12), Dec 1985.

[17] Hennessy K., Badolato A., Winger M., Gerace D., Atature M., Gulde S., Falt S., Hu E. L., and Imamoglu A. Quantum nature of a strongly coupled single quantum dot-cavity system. *Nature*, 445(7130):896–899, Feb 2007.

[18] David Press, Stephan Götzinger, Stephan Reitzenstein, Carolin Hofmann, Andreas Löffler, Martin Kamp, Alfred Forchel, and Yoshihisa Yamamoto. Photon Antibunching from a Single Quantum-Dot-Microcavity System in the Strong Coupling Regime. *Phys. Rev. Lett.*, 98:117402, Mar 2007.

[19] S. Rudin and T. L. Reinecke. Oscillator model for vacuum Rabi splitting in microcavities. *Phys. Rev. B*, 59:10227–10233, Apr 1999.

[20] Brown R. Hanbury and Twiss R. Q. Correlation between Photons in two Coherent Beams of Light. *Nature*, 177(4497):27–29, Jan 1956. 10.1038/177027a0.

[21] S. Reitzenstein. Semiconductor Quantum Dot #x2013;Microcavities for Quantum Optics in Solid State. *Selected Topics in Quantum Electronics, IEEE Journal of*, 18(6):1733–1746, Nov 2012.

[22] C. C. Gerry and P. L. Knight. *Introductory Quantum Optics*. Cambridge University Press, 2004.

[23] J. D. Joannopoulos, S. G. Johnson, J. N. Winn, and R. D. Meade. *Photonyc Crystals: Molding the flow of light* . Princeton University Press, second edition, 2008.

[24] Alexey V. Kavokin, Jeremy J. Baumberg, Guillaume Malpuech, and Fabrice P. Laussy. *Microcavities*. Oxford University Press., 2007.

[25] Asher Peres. Separaility criterion for Density Matrices. *Phys. Rev. Let.*, 77(8), Aug 1996.

[26] Ryszard Horodecki, Paweł Horodecki, Michał Horodecki, and Karol Horodecki. Quantum entanglement. *Rev. Mod. Phys.*, 81:865–942, Jun 2009.

[27] Scott Hill and William K. Wootters. Entanglement of a Pair of Quantum Bits. *Phys. Rev. Lett.*, 78:5022–5025, Jun 1997.

[28] Jürgen Audretsch. *Entangled systems: new directions in quantum physics*. Wiley-CVH, 2007.

[29] Roy J. Glauber. The Quantum Theory of Optical Coherence. *Phys. Rev.*, 130:2529–2539, Jun 1963.

[30] Elena del Valle Reboul. *Quantum Electrodynamics with Quantum Dots in Microcavities.* PhD thesis, Feb 2009.

[31] Leslie E. Ballentine. *Quantum Mechanics: A Modern Development*. World Scientific, 1998.

[32] Walter Greiner, Ludwig Neise, and Horst Stöcker. *Thermodynamics and Statistical Mechanics*. Springer, 2004.

[33] H. J. Carmichael. *Statistical Methods in Quantum Optics 1,2*. Springer, 2002.

[34] G. W. Gardiner. *Quantum Noise*. Springer-Verlag, 1991.

[35] S. Haroche and J. M. Raimond. *Exploring the Quantum: Atoms, Cavities, and Photons*. Oxford University Press., 2006.

[36] J. M. Villas-Bôas, A. O. Govorov, and Sergio E. Ulloa. Coherent control of tunneling in a quantum dot molecule. *Phys. Rev. B*, 69:125342, Mar 2004.

[37] Th. Forster. 10th Spiers Memorial Lecture. Transfer mechanisms of electronic excitation. *Discuss. Faraday Soc.*, 27:7–17, Apr 1959.

[38] Ahsan Nazir, Brendon W. Lovett, Sean D. Barrett, John H. Reina, and G. Andrew D. Briggs. Anticrossings in Förster coupled quantum dots. *Phys. Rev. B*, 71:045334, Jan 2005.

[39] Evangelos Voutsinas, Andreas F. Terzis, and Emmanuel Paspalakis. Control of indirect exciton population in an asymmetric quantum dot molecule. *Physics Letters A*, 378(3):219–225, Jan 2014.

[40] Paulo C Cárdenas, Nicolás Quesada, Herbert Vinck-Posada, and Boris A Rodríguez. Strong coupling of two interacting excitons confined in a nanocavity–quantum dot system. *Journal of Physics: Condensed Matter*, 23(26):265304, Jun 2011.

[41] H. S. Borges, L. Sanz, J. M. Villas-Bôas, and A. M. Alcalde. Robust states in semiconductor quantum dot molecules. *Phys. Rev. B*, 81:075322, Feb 2010.

[42] M. M. Santos, F. O. Prado, H. S. Borges, A. M. Alcalde, J. M. Villas-Bôas, and E. I. Duzzioni. Using quantum state protection via dissipation in a quantum-dot molecule to solve the Deutsch problem. *Phys. Rev. A*, 85:032323, Mar 2012.

[43] Fabrice P. Laussy, Elena del Valle, and Carlos Tejedor. Strong Coupling of Quantum Dots in Microcavities. *Phys. Rev. Lett.*, 101:083601, Aug 2008.

[44] J. I. Perea, D. Porras, and C. Tejedor. Dynamics of the excitations of a quantum dot in a microcavity. *Phys. Rev. B*, 70:115304, Sep 2004.

[45] Elena del Valle. Steady-state entanglement of two coupled qubits. *J. Opt. Soc. Am. B*, 28(2):228–235, Feb 2011.

[46] E. del Valle and F. P. Laussy. Regimes of strong light-matter coupling under incoherent excitation. *Phys. Rev. A*, 84:043816, Oct 2011.

[47] P. R. Eastham and P. B. Littlewood. Bose condensation of cavity polaritons beyond the linear regime: The thermal equilibrium of a model microcavity. *Phys. Rev. B*, 64:235101, Nov 2001.

[48] Karol Życzkowski, Paweł Horodecki, Anna Sanpera, and Maciej Lewenstein. Volume of the set of separable states. *Phys. Rev. A*, 58:883–892, Aug 1998.

[49] Michael A. Nielsen and Isaac L. Chuang. *Quantum Computation and Quantum Information*. Cambridge University Press, 2000.

[50] John Weiner and P. T. Ho. *Light-Matter Interaction*. Wiley-Interscience, 2003.

[51] J. M. Gérard, B. Sermage, B. Gayral, B. Legrand, E. Costard, and V. Thierry-Mieg. Enhanced Spontaneous Emission by Quantum Boxes in a Monolithic Optical Microcavity. *Phys. Rev. Lett.*, 81:1110–1113, Aug 1998.

[52] M. Bayer, T. L. Reinecke, F. Weidner, A. Larionov, A. McDonald, and A. Forchel. Inhibition and Enhancement of the Spontaneous Emission of Quantum Dots in Structured Microresonators. *Phys. Rev. Lett.*, 86:3168–3171, Apr 2001.

[53] Brendon W. Lovett, John H. Reina, Ahsan Nazir, Beeneet Kothari, and G.Andrew D. Briggs. Resonant transfer of excitons and quantum computation. *Physics Letters A*, 315(1–2):136–142, Aug 2003.

COLOPHON

This document was typeset using the typographical look-and-feel `classicthesis` developed by André Miede. The style was inspired by Robert Bringhurst's seminal book on typography "*The Elements of Typographic Style*". `classicthesis` is available for both LaTeX and LyX:

http://code.google.com/p/classicthesis/

Happy users of `classicthesis` usually send a real postcard to the author, a collection of postcards received so far is featured here:

http://postcards.miede.de/

VISTO BUENO

Asesor del trabajo.

Bogotá, November 2015

Ph.D. Herbert Vinck Posada